Effect of pendant distribution on the dispersancy of maleated ethylene propylene

by

Andrea Francisca Araya Salazar

A thesis
presented to the University of Waterloo
in fulfillment of the
thesis requirement for the degree of
Master of Science
in
Chemistry

Waterloo, Ontario, Canada, 2011

AUTHOR'S DECLARATION

I hereby declare that I am the sole author of this thesis. This is a true copy of the thesis, including any required final revisions, as accepted by my examiners.

I understand that my thesis may be made electronically available to the public.

ABSTRACT

This study describes how changes made to the modification of a polyolefin affect the solution properties of these modified polyolefins in apolar solvents. The modified polyolefins of interest are maleated ethylene-propylene random copolymers (EP-MAH) reacted with *N*-phenyl-*p*-phenylenediamine (NP$_3$D) to yield NP$_3$D-EP-MAH. NP$_3$D-EP-MAH is used as a dispersant by the oil-additive industry and solution properties such as self-aggregation, rheological behaviour, and its efficiency at stabilizing carbon black particles (CBPs) were investigated. The maleation of the polyolefin was characterized in terms of succinic anhydride (SAH) content and level of SAH clustering along the polymer backbone by FT-IR and UV-Vis absorption and steady-state and time-resolved fluorescence. The self-aggregation of the modified polyolefins was characterized in hexane by replacing NP$_3$D with 1-pyrenemethylamine and using fluorescence to probe excimer formation between an excited and a ground-state pyrene. The rheological behaviour exhibited by the solutions of modified polyolefins was characterized from the viscosity profiles of the solutions obtained as a function of polymer concentration. Finally, the adsorption of the modified polyolefins onto CBPs was characterized by analysis of Langmuir isotherms, which yields both the equilibrium constant and the maximum coverage for the binding of the modified polyolefins onto CBPs. The conclusions reached in this thesis are that clustering of the SAH pendants along the EP backbone enhances the ability of the modified polyolefin to self-aggregate in apolar solution. In turn, self-aggregation led to enhanced thickening of the NP$_3$D-EP-MAH solutions and stronger adsorption onto CBPs. This thesis establishes how the level of SAH clustering affects self-association and establishes its consequence on the rheological properties and adsorption isotherms of NP$_3$D-EP-MAH samples in apolar solvents.

ACKNOWLEDGEMENTS

This thesis would not have been possible without the input of my supervisor, Dr. Jean Duhamel, who guided me towards the completion of this interesting work. My greatest gratitude goes to my committee members: Dr. Mario Gauthier for gaving me insights on the fascinating world of polymers. Dr. Joao Soares for his assistance, especially in the experimental facilities needed for the achievement of this work. Dr. Mike Chong for his suggestions and advice for some chemical reactions.

I express my sincere gratitude to the University of Waterloo and to $(GWC)^2$ for accepting me as an M. Sc. student and DSM for supporting me financially, providing me with the opportunity to be part of such an important project that helps in the improvement of the environment.

I would also like to thank Cathy van Esch for her kind assistance during these two years. My thanks also go to my colleagues in the Duhamel and Gauthier laboratories, in particular to Shaohua Chen and Mike Fowler for their patient and unselfish help on how to understand the theoretical and experimental parts of this study.

Last but not least, my parents Monica Salazar and Pablo Araya for giving me the strength and support to never give up or throw in the towel. Finally, I would also like to thank my Uncle David Pickler and friends Marbella Herrera and Thomas Lutz for always being there in the difficult and happy moments. Thank you so much Dear Lord.

TABLE CONTENTS

LIST OF FIGURES

LIST OF SCHEMES

LIST OF TABLES

LIST OF SYMBOLS AND ACRONYMS

CBPs : Carbon black particles

CRPs : Carbon rich particles

DETA: Diethylene triamine

EP: Ethylene-propylene copolymer

EP-MAH: Maleated ethylene-propylene copolymer

FT-IR : Fourier transform infrared

ΔG : Gibbs free energy

I_E: Total excimer fluorescence intensity obtained from the emission spectrum of the pyrene-

labeled polymer

I_E/I_M: Excimer to monomer fluorescence intensity ratio

I_M: Total monomer fluorescence intensity obtained from the emission spectrum of the pyrene-

labeled polymer

k_{-1}: Rate constant of excimer dissociation

M_n: Number-average molecular weight

M_W: Weight-average molecular weight

M_w/M_n : Polydispersity index

M_z: Z-averaged molecular weight

MAH: Maleic anhydride

P_A: Peak-to-valley ratio for the pyrene absorbance

PEHA: Pentaethylene hexamine

PIB: Polyisobutylene

PIBSI: Polyisobutylene succinimide

PMA: 1-Pyrenemethylamine

Py: The pyrene chromophore

Py*: The excited pyrene group

Py-EP-MAH: Pyrene-labeled polymer

NMR: Nuclear magnetic resonance

NP_3D: N-Phenyl-p-phenylenediamine

NP_3D-EP-MAH: Modified ethylene-propylene copolymer

NP_3D-Su: N-Phenyl-p-phenyleneaminesuccinimide

REX: Reactive extrusion

SAH: Succinic anhydride

THF: Tetrahydrofuran

UV: Ultraviolet

λ_{em}: Emission wavelength

λ_{ex}: Excitation wavelength

λ_{py}: Pyrene content

λ_{NP3D}: N-Phenyl-p-phenylenediamine content

λ_{SAH}: Succinic anhydride content

τ: Excited state lifetime

$1/\tau_E$: Rate constant of the excimer emission

$1/\tau_M$:: Rate constant of the monomer emission

K: Binding equilibrium constant

Γ_{max}: Maximum adsorption of the dispersant onto carbon black particles

CHAPTER 1:   INTRODUCTION

1.1 Lubricant Additives

In recent years, the ability of additives to improve the lubricating capacity and durability of the oil used in engines has been studied in a number of publications.[1-4] Lubricant additives are chemicals, organic or organometallic in nature, that are added to oils in small quantities (a few weight percents). During the operation of the internal combustion engine, oils are exposed to combustion products which, inevitably, contribute to their contamination. Contaminants typically found in engine oils include soot resulting from inefficient fuel combustion, wear debris, unburned fuel, breakdown products of base oil, corrosion products, debris from microbiological decomposition of the oil, etc. This project focuses on the study of dispersants, which are used to stabilize carbon-rich particles (CRPs) generated in the engine oil.

The internal combustion engine generates CRPs by pyrolysis or incomplete combustion of hydrocarbons.[5] Two types of carbon deposits are formed in the engine. The first type is formed by deposition on the walls of the engine cylinders and is known as pyrocarbon[5] while the second type is formed in the gaseous phase and is termed soot.[5] Soot formation is a consequence of the encounter of CRPs and their merger into larger CRPs, having sizes ranging between 100 and 1,000 nm.[6] In a recent paper, Herd and coworkers[7] have classified CRPs into four easily distinguishable shape categories which are described in Figure 1.1.

| TYPE 1 : SPHEROIDAL | TYPE 2 : ELLIPSOIDAL |
| TYPE 3 : LINEAR | TYPE 4 : BRANCHED |
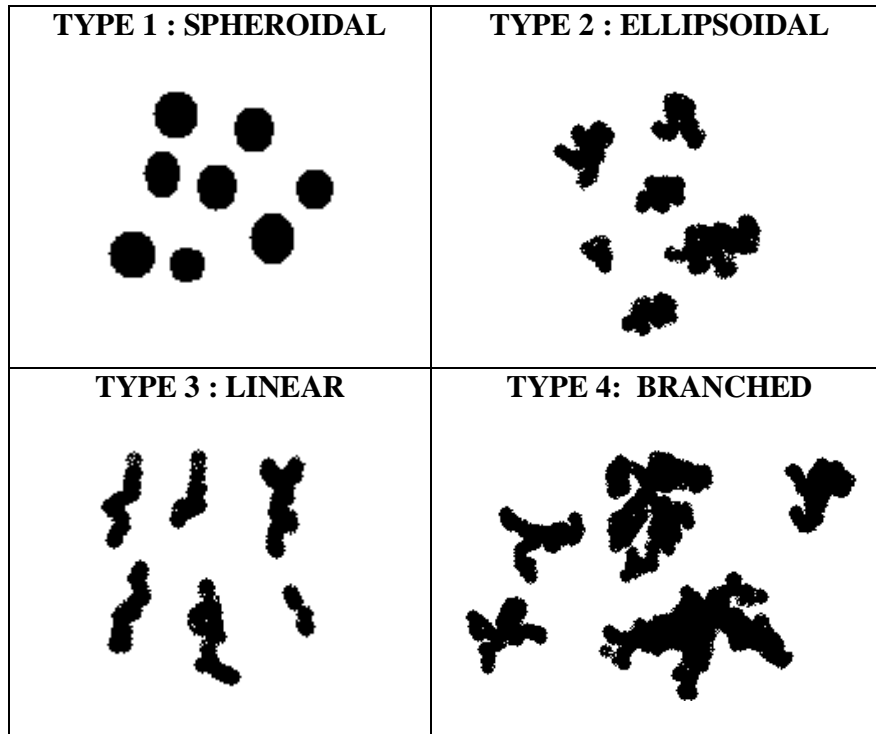
Figure 1.1: Shape categories for carbon-rich particles.[7]

The agglomeration of CRPs can damage engines since aggregated CRPs block the oil supply or even the filters. Currently, there is an ongoing debate by federal environmental agencies[8] with a mandate to protect the environment on how to reduce CRP emissions into the environment. In addition to their contribution to global warming,[9] CRPs also speed up melting of snow and ice and are probably partly responsible for the rapid melting of the world's glaciers.[9] CRPs in the atmosphere cause regional haze that depresses plant productivity[10] and constitute a significant health hazard, as it is responsible for a number of ailments that include headaches, dizziness, sleepiness, nausea, irritated eyes, breathing difficulties, respiratory problems (such as cancer and coughing).[11-12] One solution to many of these problems would be to use oil additives to reduce CRP emission.

The primary functions of oil additive are to neutralize any acid formed during fuel combustion, prevent lacquer and varnish formation on the operating parts of the engine, and prevent the flocculation or agglomeration of particles into carbon deposits which may choke the flow of the oil ways. Dispersants constitute a family of oil additives [13] which can be divided into two categories depending on whether they are mild dispersants or over-based (alkaline) dispersants.[14] Mild dispersants are usually apolar polymers modified with a small number of polar pendants that can adsorb onto the surface of colloidal particles which remain suspended in the oil thanks to the apolar chain. This process is depicted in Figure 1.2.
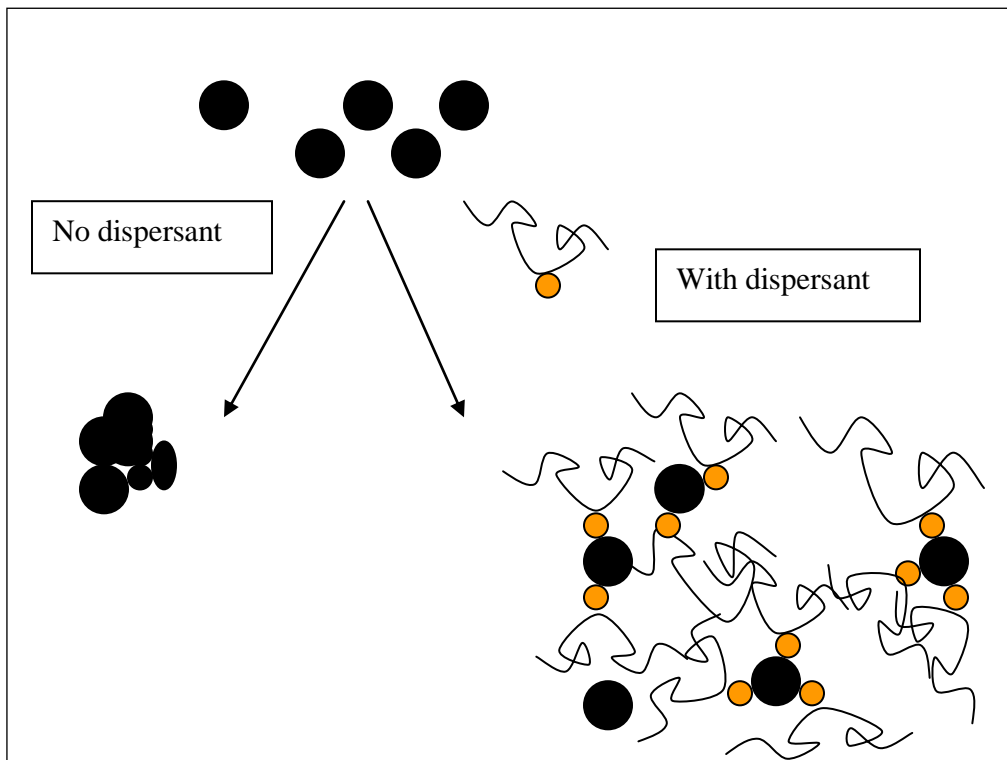
Figure 1.2: Aggregation or prevention of aggregation for carbon-rich particles in an engine in the absence (left) or presence of dispersant (right).

Polyisobutenes, polyisoprene, polypropylene, polydecene and other alkene-based copolymers[15] are used to prepare mild dispersants. These dispersants are referred to as ashless dispersants because they do not contain metal ions and thus, do not generate ashes during combustion. Furthermore, they are amphiphilic polymers that stabilize polar particles in oil via a steric mechanism described hereafter. Upon adsorption of the polar pendants of the dispersant onto the surface of the CRPs, the apolar chain of the dispersant remains solvated and disordered. When two particles coated with dispersant approach one another, interpenetration of the dispersant layer occurs resulting in a loss of disorder and a decrease in the entropy of the system which is not energetically favoured. Thus an encounter between particles stabilized by a dispersant is entropically disfavored. As a result, adsorption of a dispersant onto the CRP surface favors interparticular repulsion between two coated particles, resulting in their stabilization. Although this phenomenon has been extensively investigated, the effect that different parameters such as the nature of the adsorbed polymer, the adsorbate, or the solvent have on the strength of adsorption have not been investigated.[16] In fact, the basic mechanism for the stabilization of CRPs by adsorption of a dispersant is still under investigation with steric stabilization having been suggested as a possible mechanism.[17]

Ashless dispersants are often prepared with polyolefins that are functionalized by attaching reactive groups onto their backbone. In this respect, the grafting of polyolefins with maleic anhydride (MAH) has received much attention due to their large number of applications.[18] Maleated EP copolymers (EP-MAH) are further modified to enhance their ability to self-assemble in solution or adsorb onto CRPs by reacting the SAH pendants with amine-rich chemicals such as aminecarbazole, amineindole, aminomercaptotriazole, and more importantly for this thesis, *N*-phenyl-*p*-phenylenediamine (NP$_3$D).[19] This project is to study the efficiency an

EP-MAH that was modified with NP_3D at stabilizing CBPs in an apolar solvent. The binding of the modified ethylene-propylene copolymer (NP_3D-EP-MAH) onto CBPs was characterized by the analysis of Langmuir isotherms to yield both the equilibrium constant and the maximum coverage for the binding of the dispersant onto CBPs.

1.2 Carbon black particles (CBPs) as a relevant model for carbon rich particles (CRPs)

Carbon black (CB) has been shown to be a good model for diesel soots, even though CB and engine soot are known to have different physical properties.[20] CB is a strongly adsorbent material that is inexpensive. Its physical and chemical properties such as porosity, particle size, degree of oxidation and even the oxidized group functionality (acidic or basic in nature) can be altered by adjusting the combustion process or by post-manufacture chemical treatment.[21]

CB suspensions in aliphatic solvents generally aggregate to form agglomerates in a process referred to as cluster-cluster aggregation.[22-23] In general, two different limiting aggregation regimes are distinguished. The first one is called Diffusion Limited Colloidal Aggregation (DLCA). Aggregation occurs rapidly via the diffusive encounters of different clusters. The second one, called Reaction Limited Colloidal Aggregation (RCLA), corresponds to an aggregation that occurs more slowly due to repulsive forces that limit the aggregation. Since a repulsive short-range energy barrier exists between clusters when they approach one another, a large number of collisions are required before two clusters can join together.[23]

Bezot et al.[24] described the aggregation kinetics of carbon black particles in oil in the presence of olefinic copolymers and an ashless dispersant (polyisobutylene succinimide). Light scattering provides information on the variation of the mean effective radius of a cluster as a function of time. A good dispersant maintains this radius as small as possible for a long period of time as it

inhibits aggregation of the carbon black particles. The experiments conducted by Bezot et al. showed how the kinetics of aggregation are slowed down when a modified polymer acting as a dispersant is used. This effect is illustrated in Figure 1.3 where the growth of the cluster radius is reduced significantly upon using a polyisobutylene (PIB) modified at one end with a succinimide group.
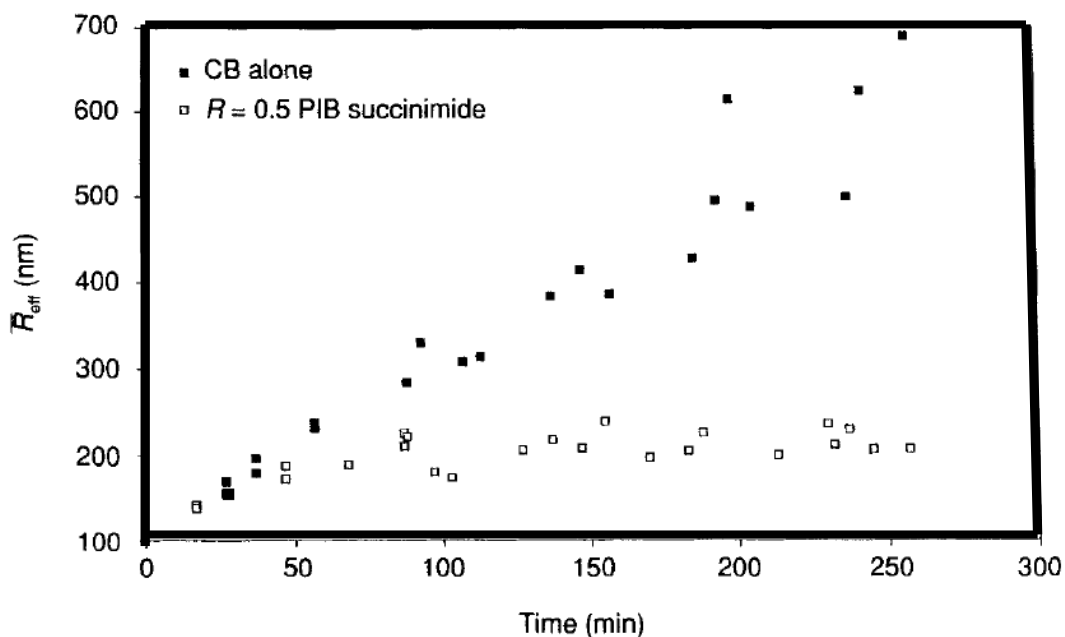
Figure 1.3: Time dependence of the mean effective cluster radius with (☐) or without (■) PIB succinimide. Figure taken from Reference # 24.

1.3 Mechanism for the stabilization of CRPs

Adsorption of a dispersant onto a CRP occurs at the interface between a solid CRP and the solvent. Generally, this region is referred to as a boundary between two immiscible phases where the chemical and physical characteristics of one bulk phase change abruptly to become those of the other phase.[25] Two basic interactions are usually considered, one being attractive and the

other repulsive. When attraction dominates, the particles will adhere and the dispersion may coalesce. When repulsion dominates, the system will remain in a dispersed state.

Van der Waals' attractive forces are always present between particles having similar composition. Therefore, a colloidal dispersion can only be stable when a sufficiently strong repulsive force counteracts the van der Waals' attraction. The repulsion between particles arises usually from two different sources, one being repulsion due to the interaction between electrical double layers (or surface charges) on the particles, and the other being a repulsion due to the interaction between adsorbed layers of nonionic material. These two basic mechanisms which are important for the stabilization of colloidal dispersions are termed electrical stabilization and steric stabilization, respectively.[26]

Many theories have been proposed to explain the steric stabilization mechanism.[27-28] One of these theories involves entropic stabilization. It assumes that a second surface approaching the adsorbed layer is impenetrable. Thus the approaching impenetrable surface compresses the adsorbed layer and the polymer segments located at the interface lose configurational entropy ($\Delta S < 0$). This reduction in entropy makes the change in Gibbs free energy more positive ($\Delta G = \Delta H - T\Delta S$) reducing the likelihood of particle encounter. In effect, the particles with adsorbed polymeric dispersants repel each other, preventing the particles from flocculating and resulting in their stabilization in solution

1.4 Effect of pendant distribution on the dispersancy of maleated EP copolymers

Various chemical and technological routes have been developed for producing maleated EP copolymers. From a chemical perspective, the most common procedure involves free radical

grafting induced by mainly peroxide radical initiators, but also by oxygen, mechanical degradation under shear, or irradiation with high energy particles.[29]

Most maleated polyolefins are used as interfacial agents thanks to their chemical composition that combines polar groups and an apolar chain. Therefore, maleated poyolefins are employed to enhance the adhesion of a polyolefin to polar materials made of polar synthetic polymers (polyamides, polyesters) and inorganics (metals, glass, silica, talcum) and natural polymers (wood and cellulose in paper). Enhanced adhesion results from the increased polarity of the polyolefin upon grafting with MAH, but more importantly to the chemical reactivity of the grafted MAH unit towards a wide range of other compounds bearing varied functionalities (amine, amide, alcohol and metal oxide).[30] In particular, when maleated EP copolymers are reacted with a primary amine to yield succinimide groups, the product of this reaction is used as an additive for motor oils where it acts as a viscosity modifier and particle stabilizer.[31]

The grafting of MAH onto polyolefins is usually performed in the melt with mixing equipment that is typically used with thermoplastics such as kneaders or extruders, depending on whether the process is carried out batchwise or continuously, respectively.[30] The main advantage of reactive extrusion (REX) over grafting in solution is that no solvent is involved, an aspect which is beneficial from both cost and environmental perspectives. Other advantages of REX include good mixing efficiency, flexible operation, and ease of development and scale-up. Despite the numerous advances made in the production of maleated EP copolymers, little is known about the distribution of the succinate groups grafted onto EP copolymers.

In this study, the microstructure of maleated EP copolymers refers to the distribution of the succinic anhydride (SAH) units along the EP backbone (Figure 1.4). SAH units can be found as clustered, isolated, or oligomeric units.[32]
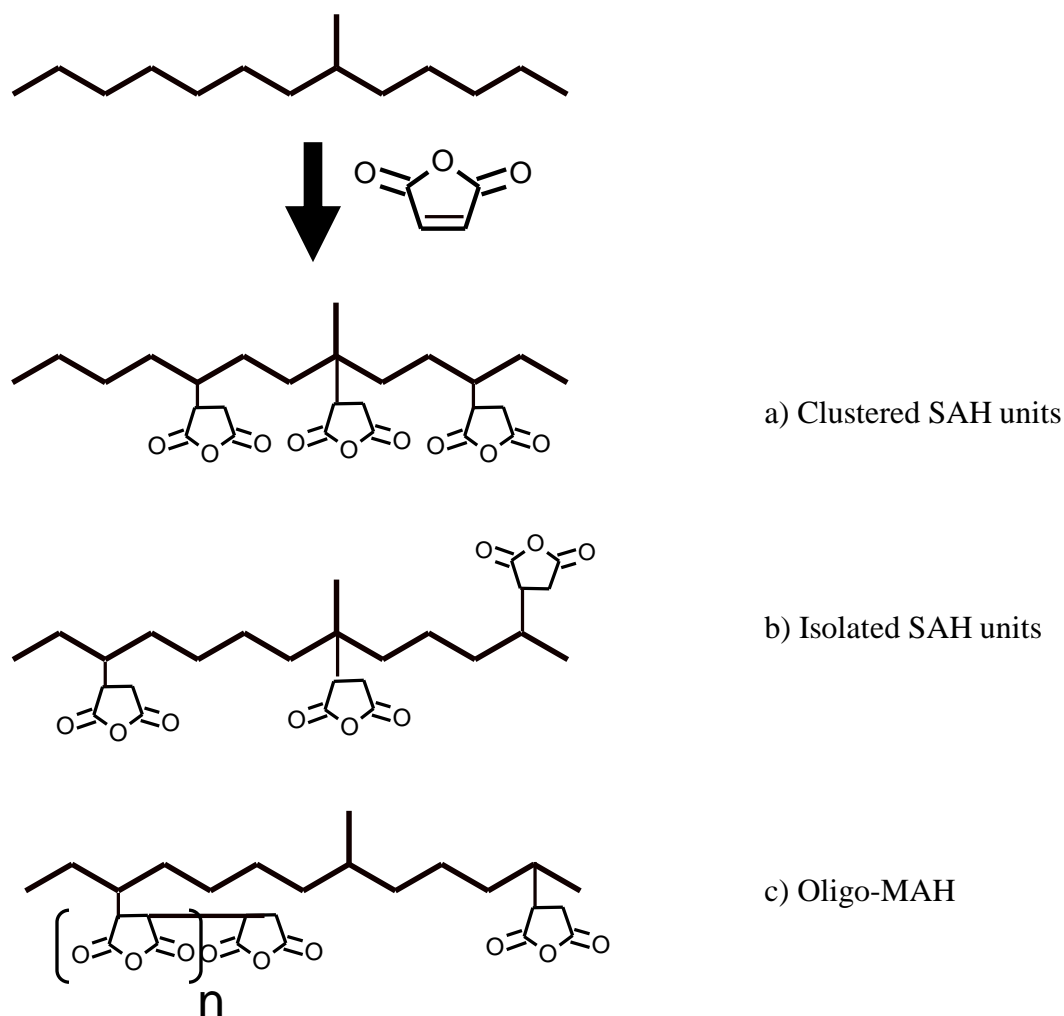
Figure 1.4: Microstructure of maleated EP copolymers.[30]

    To date, information on the level of SAH clustering of a maleated EP copolymer can only be inferred from the steep increase in viscosity of an EP-MAH solution in apolar solvents with increasing EP-MAH concentration. This steep viscocity increase is due to the formation of an interpolymeric network held together by polar SAH aggregates. Interestingly, clustering of the SAH pendants along the EP backbone induces stronger polymeric aggregation, resulting in a steeper increase of solution viscosity with polymer concentration.[33,34] Unfortunately, these viscosity experiments only yield qualitative information on the level of SAH clustering of

maleated EP copolymer. In contrast, Duhamel's laboratory has shown that fluorescence experiments conducted on maleated EP copolymers labeled with pyrene provide a direct measure of the level of SAH clustering of maleated EP copolymers, which was applied to establish the effect that SAH clustering has on the self-association of EP-MAH, and its consequence on the reological behavior and adsorption efficiency of modified EP-MAH in apolar solution.

1.5 Organization of the thesis.

The purpose of this study was to expand the scope of previous studies conducted in the Duhamel laboratory on the characterization of the behavior of maleated ethylene-propylene copolymers (EP-MAH) in solution.[35] Seven EP-MAH samples were characterized and their behavior in solution was investigated. Since, NP_3D-EP-MAH acts as a viscosity modifier and colloidal stabilizer in solution, this work focused on characterizing the effect of succcinic anhydride (SAH) clustering on the rheological behavior of NP_3D-EP-MAH solutions and the binding efficiency of EP-NP_3D onto carbon black particles (CBPs).

After a general introduction on the research topic presented in Chapter 1, the experimental procedures used in this thesis are described in Chapter 2. The characterization of the EP-MAH copolymer in terms of molecular weight distribution, SAH content and level of SAH clustering are described in Chapter 3. The effect of SAH clustering on the solution behavior of NP_3D–EP-MAH is discussed in Chapter 4. Finally, the conclusions of this study are presented in Chapter 5 with suggested future work.

CHAPTER 2: EXPERIMENTAL SECTION

2.1 Maleated ethylene-propylene copolymers

Seven samples of maleated ethylene-propylene copolymers (EPX-MAH), where X=1-7, were provided by DSM. The seven EPX-MAH samples were labeled with 1-pyrenemethylamine (PMA) to determine their level of SAH clustering. Since EP1-MAH and EP7-MAH have the same SAH content and level of SAH clustering on the one hand and EP2-MAH, EP4-MAH, and EP5-MAH were found to have both similar SAH content and level of SAH clustering, five EPX-MAH samples, namely EPX-MAH with X=3-7 were modified with *N*-phenyl-*p*-phenylenediamine and studied to determine the effect that the clustering of SAH units has on the solution properties of the capped EPX-MAH samples. The chemical structure of the two different succinimides used in this study is shown in Figure 2.1.

| 1-pyrenemethylsuccinimide | *N*-phenyl-*p*-phenyleneaminesuccinimide |
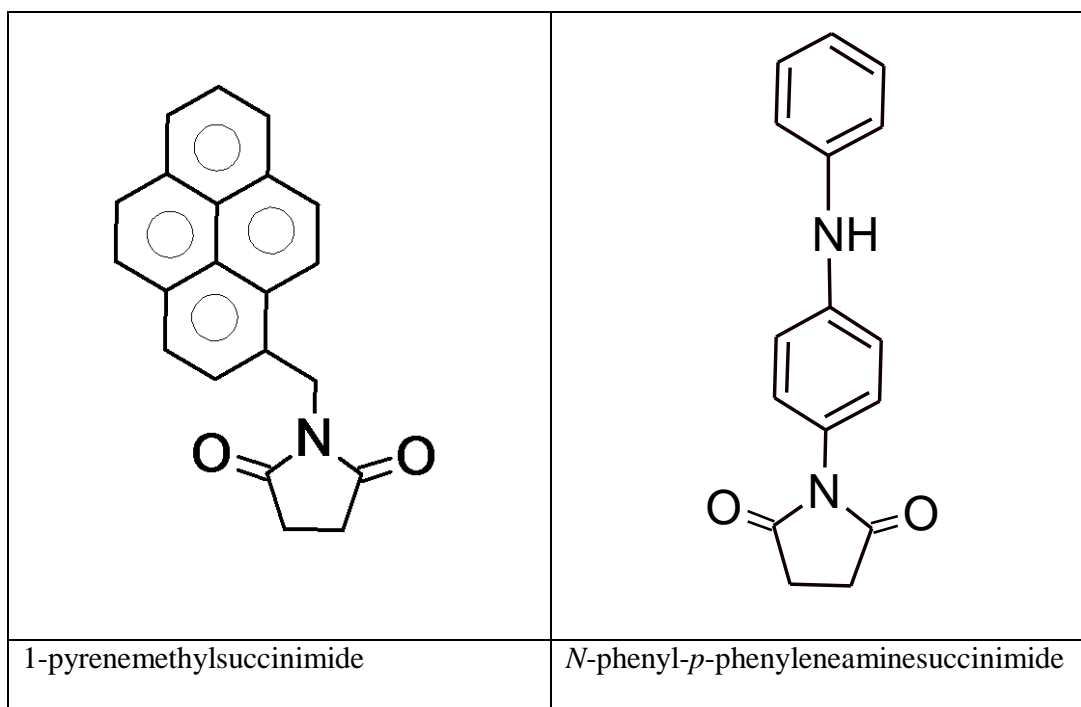
Figure 2.1: Chemical structure of the succinimides.

2.2 Materials

N-Phenyl-*p*-phenylenediamine hydrochloride, 1-pyrenemethylamine, activated carbon black (Aldrich 100-mesh powder), and anhydrous dodecane 99% were purchased from Sigma-Aldrich. PTFE filters with 0.4 μm pores were supplied by Millipore, Tetrahydrofuran (distilled in glass), methanol (HPLC grade), acetone (HPLC grade), and hexane (HPLC grade) were purchased from Caledon. Ammonium hydroxide (0.001 M) was supplied by Fisher. Glycerol was purchased from EM Science. The seven maleated EP copolymers, EPX-MAH with X= 1-7, were kindly provided by DSM (The Netherlands).

2.3 Instrumentation

2.3.1 UV-Vis

The absorption of the polymer solution was measured with a Varian 100 Bio UV-Vis spectrophotometer with a 1 cm path length UV plates.

2.3.2 FT-IR

All FT-IR spectra were acquired with a Bruker Temsor 27 FTIR spectrophotometer using NaCl solid plates by averaging 35 scans and with a 1 cm^{-1} resolution.

2.3.3 Gel Permeation Chromatography (GPC)

GPC experiments were conducted in the laboratory of Prof. Joao Soares by Dr. Saeid Mehdiabadi. A Polymer Char GPC equipped with three detectors in series (infra-red, 15° angle light scattering, and differential viscometer) was used. The solvent 1,2,4-trichlorobenzene (TCB) was used to prepare the EPX-MAH samples.

14

Analysis of the molecular weight distribution of the EPX-MAH samples was carried out according to the ASTM Standard[1] D883 and D3016 procedures at 145 $^{\circ}$C with a flow rate of TCB of 1 mL/min. The instrument was equipped with three PLgel Olexis 13 mm mixed pore columns (300 mm in length, 7.5 mm internal diameter). The range of M_w accessible with this type of column was 2000 - 7×10^6 g/mol.

2.3.4 Shaker

An Innova™ 4000 incubator shaker purchased from New Brunswick Scientific was used for the Langmuir isotherms experiments. The shaking rate was set at 350 rpm/min for 18 hours.

2.3.5 Steady-state fluorescence measurements

The fluorescence spectra of the EPX-MAH samples were obtained with a Photon Technology International LS–100 steady–state fluorometer. The solutions for fluorescence measurements were degassed for 30 minutes under a gentle flow of nitrogen. The excitation spectra were obtained using slit widths of 1 and 2 nm on the excitation and the emission monochromators, respectively. The slit widths on the excitation and emission monochromators were set to 2 and 1 nm, respectively, for the emission spectra. All fluorescence spectra were collected using the right angle geometry.

2.3.6 Time-resolved fluorescence measurements

The fluorescence decays of the EPX-MAH samples were conducted on a Photochemical Research Associate, Inc. System 2000 using the time-correlated single-photon counting (TC-SPC) technique. The EPX-MAH solutions were excited at 344 nm and the excimer decays were

acquired at 510 nm. In order to prevent residual light scattering from reaching the detector, an optical filter with a wavelength cut-off at 480 nm was used. For each sample, the instrument response functions and fluorescence decays were acquired with 20,000 counts at the maximum to ensure an adequate signal-to-noise ratio.

2.3.7 Nuclear Magnetic Resonance (NMR)

The ^{1}H NMR spectra of the samples were obtained on a Bruker 300 MHz high resolution NMR spectrometer. Deuterated dimethylsulfoxide 99.9% (DMSO) was used as the solvent.

2.3.8 Viscometer

The viscosity of the EPX-MAH solutions was measured on an Ubbelohde viscometer. The temperature was controlled with a water bath set at 25.0 ± 0.1 °C. A calibration curve correlating the known viscosity[2] of water/glycerol mixtures as a function of mixture composition was established to calculate the constant K of the viscometer found to equal 0.1007 mPa.mL.g^{-1}.

2.4 Sample preparation

2.4.1 Labeling EPX-MAH with pyrene (Py-EPX-MAH)

The labeling reaction followed the conditions described by Zhang et.al.[3] 1-Pyrenemethylamine hydrochloride (PMA-HCl) was dissolved in a mixture of 40 mL of hexane and 15 mL of aqueous solution of ammonium hydroxide (0.001 M) to deprotonate the amine. The mixture was shaken vigorously for one minute. The aqueous phase was discarded and the organic phase was collected. This procedure was repeated 7 times. The organic phase was dried with NaOH pellets before being filtered. EPX-MAH (0.55 g) was dissolved in 30 mL of

anhydrous dodecane and heated to 130 °C, as measured with a thermometer placed in the oil bath, under nitrogen for 6 h. The reaction flask was equipped with a Dean Stark apparatus and a condenser. Then 20 mL of 1-pyrenemethylamine (PMA) solution was added with the help of a pipette (drop by drop on the wall of the round-bottom flask).Then, 20 ml of THF was added to clean the wall of the round-bottom flask. A 35% molar excess of PMA was fed to the reaction flask to ensure that all the succinic anhydride (SAH) pendants would react. The reaction was allowed to proceed under reflux for 28 h at 190 °C, assumed temperature, under nitrogen. The resulting pyrene-labeled polymer (Py-EPX-MAH) was precipitated from dodecane into acetone. The polymer was purified by precipitation from hexane into methanol. The precipitation was repeated at least ten times to ensure that the polymer was completely free of unreacted PMA as verified from the analysis of the fluorescence decays of the Py-EPX-MAH samples. After the precipitation, the polymer was left in a glass bottle which was placed in a vacuum oven set at 60 ± 5 °C to remove traces of solvent. The dried polymer formed a thin film at the bottom of the bottle to enhance the removal of residual traces of solvent and water.

The presence of unreacted SAH pendants left in the polymer can be detected by monitoring the peak at 1785 cm^{-1} in the FTIR spectrum, characteristic of the SAH carbonyls. If the reaction is complete, no unreacted SAH pendant remains in the polymer sample and the peak at 1785 cm^{-1} characteristic of the SAH carbonyls is strongly reduced or even inexistent as illustrated in Figure 2.2 A. Figure 2.2 B shows a typical spectrum where the reaction was not complete. The spectrum exhibits a more pronounced absorption band at 1704 cm^{-1} characteristic of the succinimide carbonyls, which indicates that a substantial amount of unreacted SAH carbonyls remain in the sample. In addition, absorption bands at 1462 cm^{-1} and 1377 cm^{-1} represent the C-

H bends of the methylene (CH$_2$) and methyl (CH$_3$) groups, respectively. Figure 2.2 B also shows a peak at 1260 cm^{-1} characteristic of the C-O ether of the solvent tetrahydrofuran (THF).
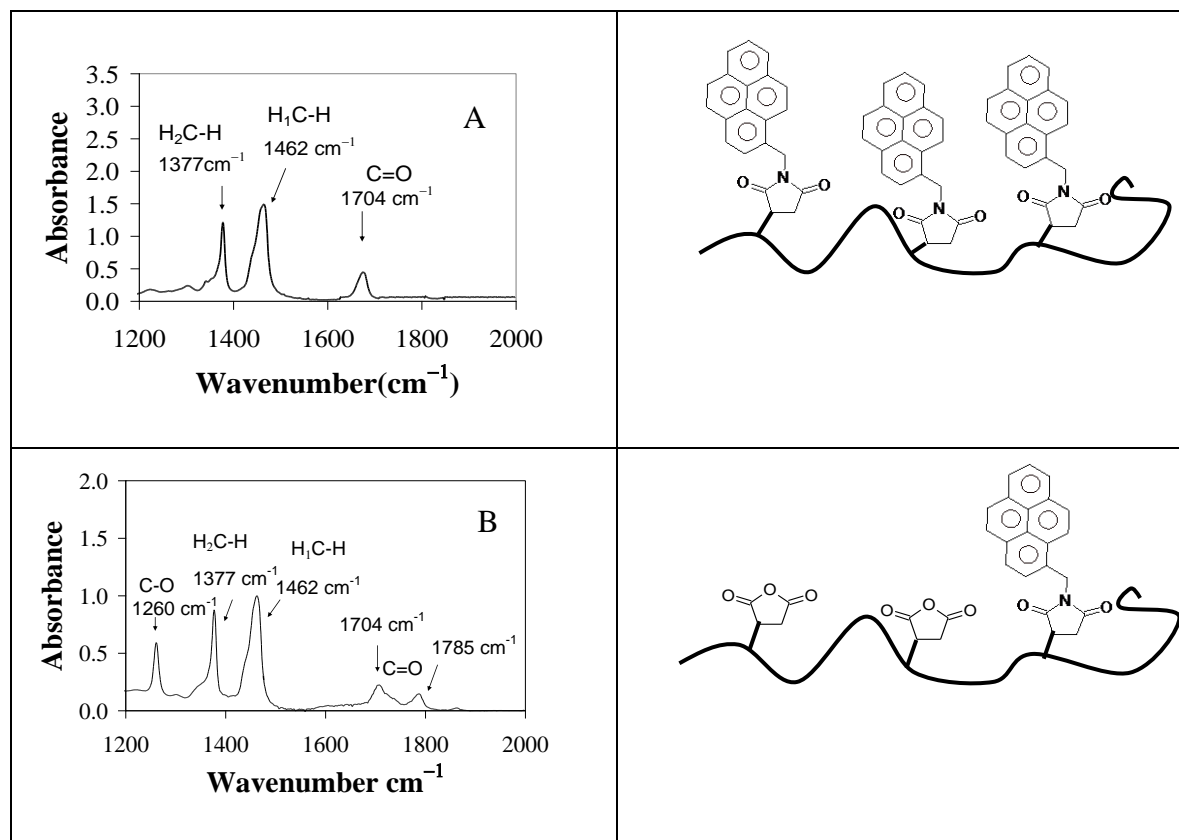
Figure 2.2: FTIR spectra corresponding to a fully (A) and partially (B) capped Py-EP5–MAH sample.

2.4.1.1 Determination of the pyrene and NP$_3$D contents of the capped EPX-MAH samples

After having established by FTIR (see Figure 2.2) that EPX-MAH was fully labeled with PMA or NP$_3$D referred to as dye (D) from now on, the dye content of the polymer was determined by measuring the absorption of the solution prepared by dissolving a carefully weighed amount, *m,* of the capped polymer (Py-EPX-MAH or NP$_3$D-EPX-MAH) in a known

18

volume, *V*, of THF. The dye concentration was then determined from the absorption value at

344 nm or 294 nm, for pyrene or NP$_3$D, respectively. The molar extinction coefficient of a model

compound, typically 1-pyrenemethylsuccinimide (ε[344 nm, in THF] = 44,500 cm^{-1} .M^{-1})^4 and

NP$_3$D-SAH (ε[294 nm, in THF] = 20,400 cm^{-1}.M^{-1}) were used. The dye content, λ_D, of Py-EPX-

MAH or NP$_3$D-EPX-MAH expressed in moles of dye per gram of polymer was calculated from

Equation 2.1.

$$\lambda_D = [D] \, V \, / \, m \qquad\qquad\qquad (2.1)$$

2.4.2 *Labeling of EPX-MAH with N-phenyl-p-phenylenediamine (NP$_3$D-EPX-MAH)*

Figure 2.3 shows a representative FTIR spectrum for a NP$_3$D-EP6-MAH sample. The

absorption bands at 1377 and 1462 cm^{-1} represent the C-H bend of the methyl (CH$_3$) and

methylene (CH$_2$) groups, respectively. The absorption bands at 1595 and 1711 cm^{-1} are

characteristic for the N-H bend and succinimide carbonyls, respectively. The two prominent

peaks around 1490 cm^{-1} are attributed to the C-N stretch of the aromatic amines.

The labeling reaction with NP$_3$D was carried out in the same manner as with PMA. The only

difference was that an 8% molar excess of NP$_3$D (instead of 35% for PAM) was enough to

ensure that all SAH pendants would be fully capped (see Figure 2.3 and 2.4 A).
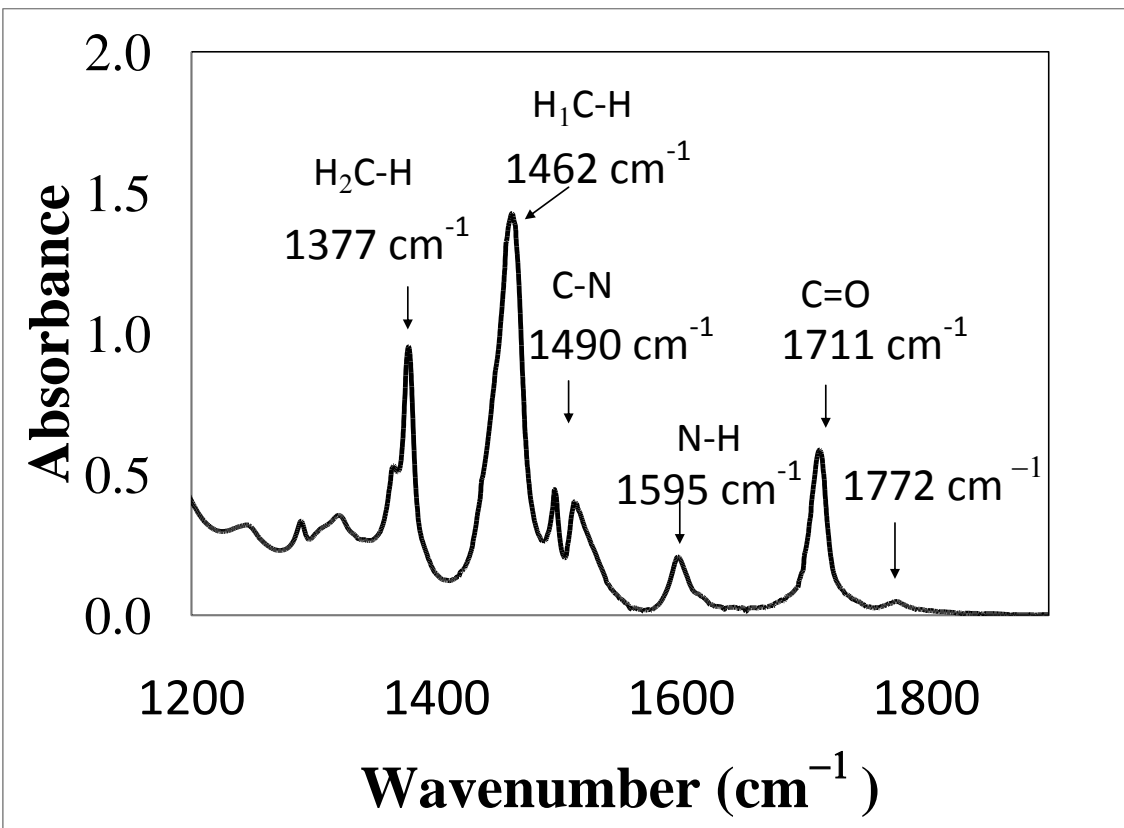
Figure 2.3: FTIR spectrum for NP$_3$D-EP6-MAH

As for the Py-EPX-MAH samples, the presence of unreacted SAH pendants in the polymers labeled with NP$_3$D could be inferred by monitoring the peaks at 1711 and 1785 cm^{-1} characteristic of the succinimide and SAH carbonyls, respectively. Strong reduction or even disappearance of the peak at 1785 cm^{-1} characteristic of the SAH carbonyls ensured that the NP$_3$D labeling reaction went to completion leading no unreacted SAH in the polymer. Figure 2.4 B shows a typical spectrum where the reaction was not complete and a more pronounced absorption band at 1785 cm^{-1} is observed.
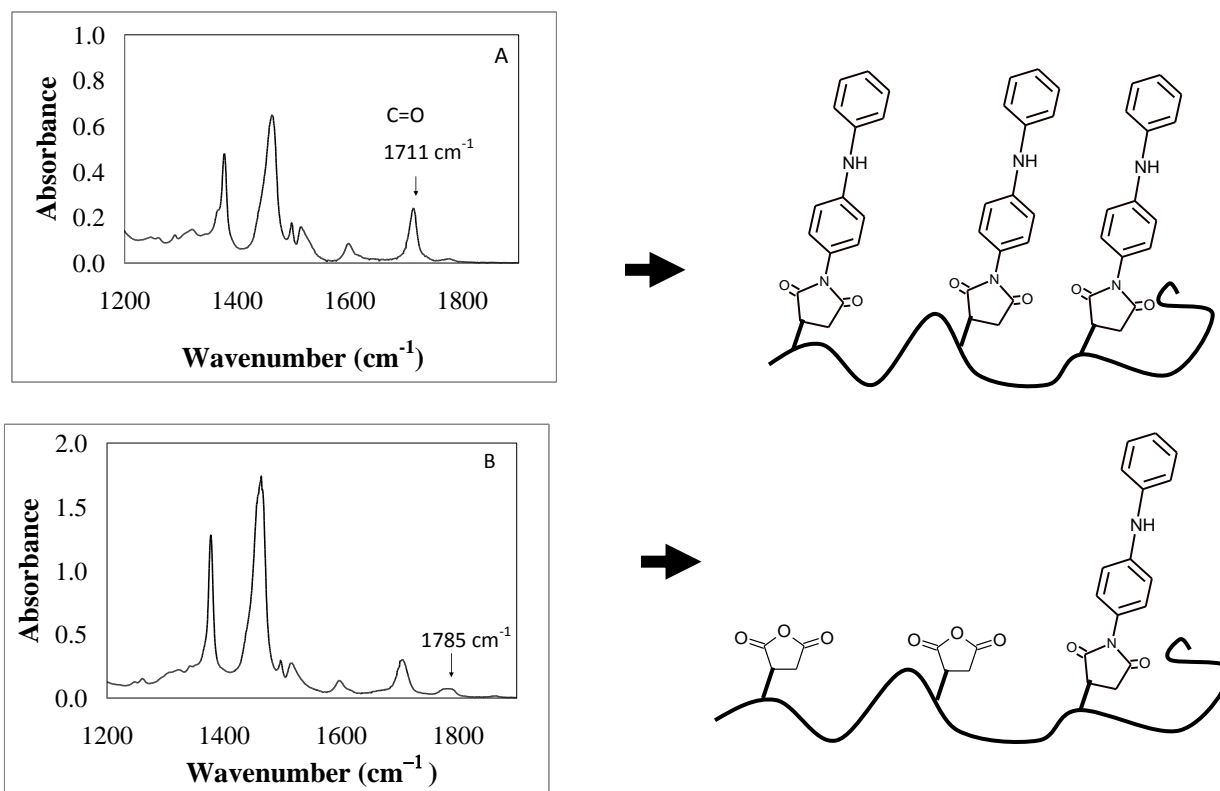
Figure 2.4: FTIR spectra of the NP$_3$D-EP3-MAH samples. A) Fully labeled, B) partially labeled

2.4.3 Synthesis of the succinimide of N-phenyl-p-phenylenediamine NP$_3$D-Su

N-Phenyl-*p*-phenylenediamine (5 g, 0.027 mol), succinic anhydride (3 g, 0.03 mol), and anhydrous sodium acetate (3.28 g, 0.04 mol) were refluxed in acetic acid (25 mL) for 5 hours at 130 °C, as recorded from a thermometer in the oil bath, to yield the succinimide of NP$_3$D (NP$_3$D-Su). The reaction mixture was then cooled to room temperature and a yellow solid precipitated. Extractions with sodium carbonate (0.1 N) removed the excess of succinic anhydride and acetic acid. Purification of NP$_3$D-Su was performed by crystallization in a 2:1 (v/v) mixture of hexane:ethyl acetate. The ^{1}H NMR spectrum of NP$_3$D-Su acquired in deuterated dimethylsulfoxide (DMSO) (99.9 %) is shown in Figure 2.5. The peaks between 6.8 and 7.24 ppm represent the aromatic protons. The amine proton **4** appears at 8.3 ppm. The peak at 2.7

21

ppm corresponds to the succinimide protons. The peaks at 3.28 and 2.46 ppm represent the water and DMSO protons, respectively. The good agreement found between the integration of the ^{1}H NMR peaks with the number of protons of NP$_3$D-Su suggests that NP$_3$D-Su was successfully synthesized.
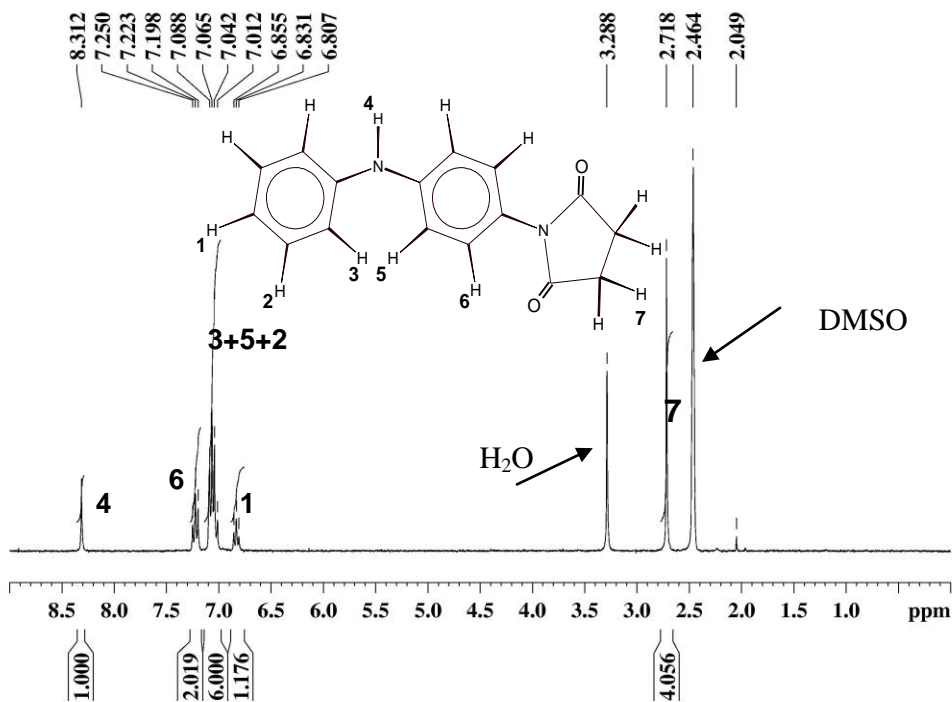
Figure 2.5: ^{1}H NMR spectrum of NP$_3$D-Su

CHAPTER 3: CHARACTERIZATION OF MALEATED   ETHYLENE-PROPYLENE COPOLYMERS

3.1 Introduction

It has been reported[1-3] that the maleation of polyolefins can be achieved in the melt by mixing the molten polymer with MAH and an initiator, such as a suitable peroxide, in an extruder at elevated temperatures. Alternatively, a solution process can also be used where the polymer dissolved in an appropriate solvent is reacted at elevated temperatures with MAH in the presence of an initiator. It is generally believed that primary free radicals generated by initiators first abstract hydrogen atoms from the polymer chain to form macroradicals. Many studies have demonstrated that cross-linking in polyethylene and chain scission in polypropylene may occur simultaneously with the graft reaction. The performance of maleated polyolefins is expected to depend on the microstructure of the grafted polymer induced by the structurally different radical sites generated by the radical initiator. The predominantly secondary and tertiary macroradicals generated in polyethylene and polypropylene, respectively, have different reactivities toward MAH. Consequently, ethylene-propylene random copolymers generate different grafting sites. Gaylord and Mehta[4] proposed that during the maleation of polyethylene, macroradicals with different average graft chain length are terminated by mostly disproportionation or hydrogen abstraction. The chemical structures of the main products expected from a grafting reaction were shown in Figure 1.4.

The properties of a modified polyolefin depend on its chemical structure which, in theory, can be characterized by several techniques. In practice however, the small amount of modification applied to a polyolefin, on usually less than 2 mol% of the backbone monomers, complicates greatly the structural characterization of modified polyolefins.

The techniques that were used in this thesis to characterize the chemical composition of the EPX-MAH samples are briefly reviewed hereafter. These techniques were used to characterize

24

seven maleated EP copolymer samples provided to us by DSM in order to determine their structure-property relationship.

3.2 Infrared Spectroscopy

Infrared spectroscopy provides information about the nature and the content of functional groups generated during the maleation of polyolefins. Figure 3.1 shows a typical FT-IR spectrum for a maleated ethylene-propylene copolymer (EP2-MAH). The symmetric stretching band of the carbonyl group occurs at different frequencies and with different band-widths at half maximum for different carbonyl-containing compounds. The characteristic carbonyl absorption band of succinic anhydride is observed in the spectrum of EP-MAH between 1780 cm^{-1} and 1800 cm^{-1}. Depending on whether isolated SAH units or oligoMAH is generated along the EP backbone, the carbonyl group of SAH is expected to absorb at 1792 cm^{-1} or 1784 cm^{-1}, respectively.[5] In addition, the characterization of the chemical composition of EP-MAH requires considering the band at 1462 cm^{-1}, characteristic of the C-H bending mode of the propylene monomer in the EP copolymer.
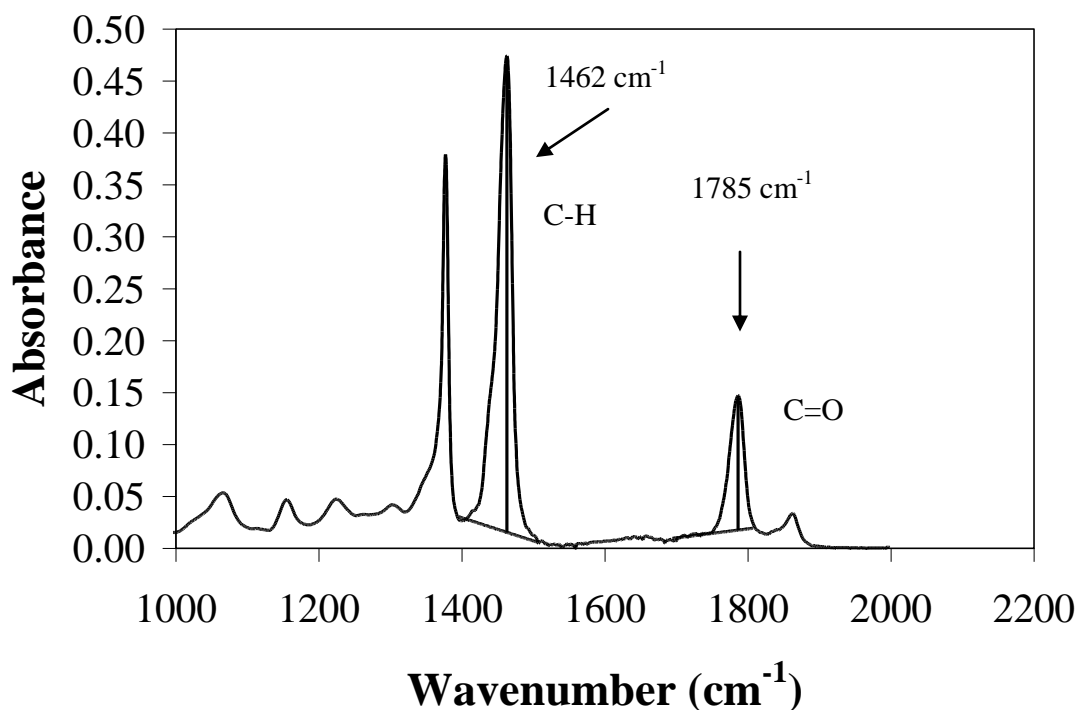
Figure 3.1: FT-IR spectrum of a maleated EP copolymer with geometrical construction to obtain peak areas and maxima.

3.3 UV-Vis Absorption

Beside FT-IR, the SAH content of EP-MAH can be determined by reacting an amine derivatized chromophore like 1-pyrenemethylamine (PMA) or N-phenyl-p-phenylenediamine (NP_3D) with the succinic anhydride pendants of EP-MAH and evaluating the chromophore content of the labeled EP-MAH by UV-Vis absorption. The EPX-MAH samples where X=1-7 provided by DSM were labeled with 1-pyrenemethylamine to yield Py-EPX-MAH according to the procedure described by Zhang et al.[6] A similar procedure was used to label the maleated EP copolymer with NP_3D.

Furthermore, UV-Vis absorption measurements of the Py-EPX-MAH samples provide a measure of the level of aggregation between the pyrene pendants by measuring the peak-to-valley ratio (P_A).[7] The P_A ratio is measured by taking the ratio of the absorbance of the peak at 344 nm to that of the nearest valley. P_A values of 3.0 or above indicate the absence of association between pyrene pendants whereas lower P_A values reflect increased pyrene association. The P_A ratio is a measure of the breadth of the peak at 344 nm. It has been found that a broader peak reflects stronger association between the pyrenyl pendants (Figure 3.2).[8]
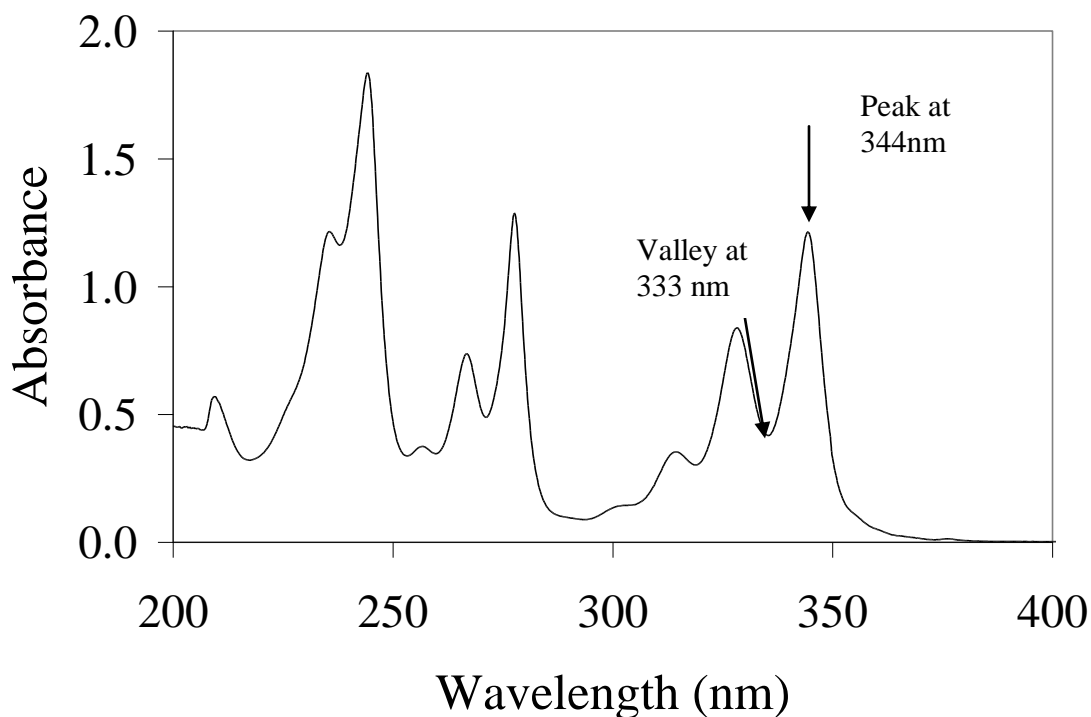
Figure 3.2: Typical absorption spectrum of Py-EP7-MAH in THF. [Poly] =0.151 g.L^{-1}, λ_{py}= 185 μmol.g^{-1}. P_A= 2.8.

3.4 Fluorescence techniques

Since the late 1970s, fluorescence techniques have been extensively applied to the study of synthetic polymers. The special photophysical properties of pyrene are particularly well suited for such studies.[7-11] In the present work, pyrene was selected for its ability to form an excimer.[7]

Excimer formation between pyrene pendants covalently attached onto a polymer is well described by the modified Birks Scheme[12] shown in Scheme 3.1. Upon absorption of a photon, an excited pyrene can either fluoresce or form an excimer[12] upon encounter with a ground-state pyrene monomer. The parameters τ_M and τ_E in the modified Birks scheme are the natural lifetimes of the pyrene monomer and excimer, respectively. If pyrene is randomly distributed along the chain of the Py-EPX-MAH samples, pyrene excimer formation by diffusion is described by the function $f(t)$, which reflects the distribution of distances spanning every two pyrenes. Excimer formation by diffusion occurs slowly. On the other hand, excimer formation between two associated pyrenes occurs instantaneously upon photon absorption. The Duhamel laboratory has shown that the difference between the time required to form an excimer, whether the pyrenes are separated or associated along the backbone, can be taken advantage of to provide quantitative information on the level of SAH clustering of EP-MAH samples.[13]
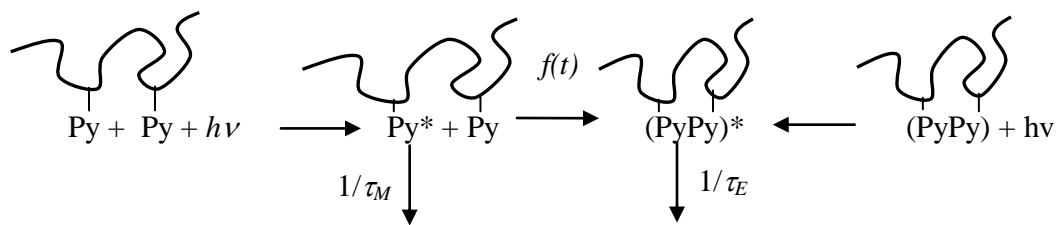
Scheme 3.1: Modified Birks' scheme illustrating diffusional excimer formation (left) and direct excitation of ground-state pyrene dimer (right) for a pyrene-labeled polymer.[12]

28

Fluorescence excimer decays provide information on the presence of ground-state pyrene dimers. Pyrene-labeled oligoMAH or clustered SAH shown as, respectively, species b) and c) in Figure 3.3 are expected to promote the formation of ground-state pyrene aggregates that form excimer instantaneously upon absorption of a photon. Excimer formation by isolated pyrenes is delayed and yields a rise time in the excimer decay. Quantification of the magnitude of the rise time in the excimer decay provides a measure of the relative amounts of excimer formed by diffusive encounters between pyrene pendants or direct excitation of pyrene aggregates. This is achieved by fitting the fluorescence decay of the excimer with a sum of exponentials and taking the ratio of the sum of the negative pre-exponential factors over the sum of the positive pre-exponential factors, namely the A_{E-}/A_{E+} ratio. The different processes expected for pyrene excimer formation in a Py-EPX-MAH solution were described in Scheme 3.1.
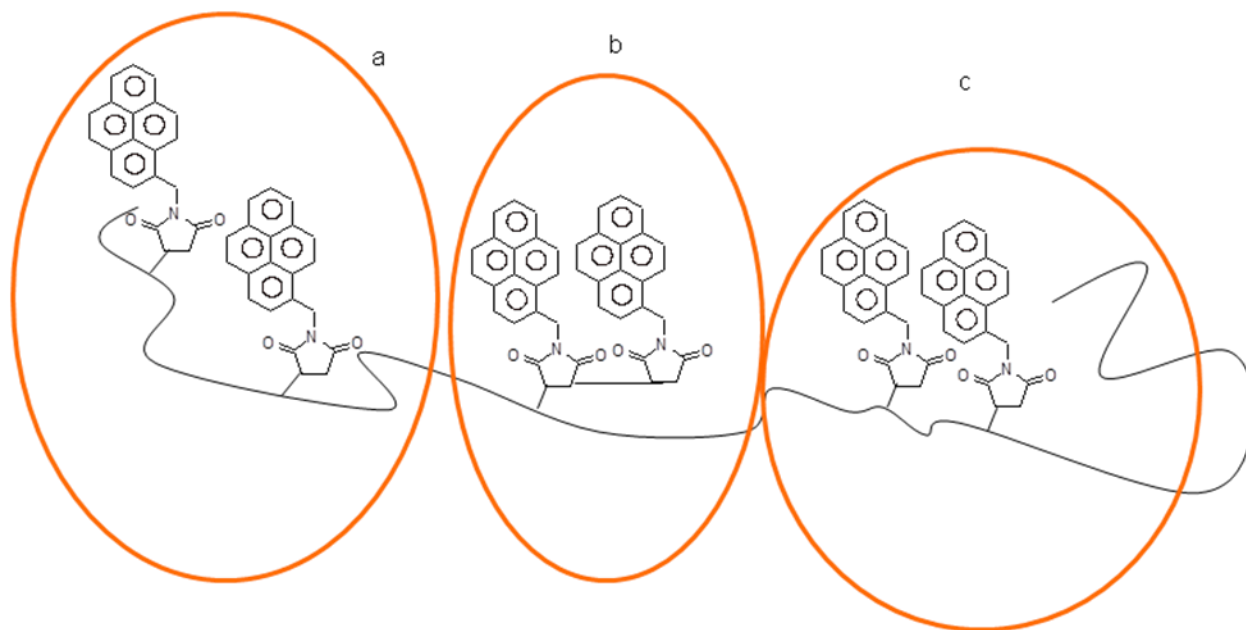
Figure 3.3: Expected chemical structure of Py-EPX-MAH: isolated SAH (a), oligo-MAH (b) or clustered SAH (c) labeled with pyrene.

3.5 Characterization of maleated EP copolymers

DSM provided seven EPX-MAH samples where X=1-7 with no prior knowledge of the grafting procedure used to prepare these samples.

3.5.1 Molecular weights

Table 3.1 lists the parameters describing the molecular weight distribution (MWD) of the Py-EPX-MAH samples obtained by Dr. Saeid Mehdiabadi in Prof. Joao Soares' laboratory. Complete capping of the SAH pendants of the EPX-SAH samples ensured minimum association of the Py-EPX-MAH samples in solution.

Table 3.1: Number-, weight-, and Z-average molecular weights and polydispersity index of the Py-EPX-MAH samples

Sample	M_n (kg/mol)	M_w (kg/mol)	M_z (kg/mol)	M_w/M_n
Py-EP1-MAH	39	85	151	2.2
Py-EP2-MAH	41	86	180	2.1
Py-EP3-MAH	40	101	237	2.6
Py-EP4-MAH	39	96	205	2.4
Py-EP5-MAH	38	83	166	2.2
Py-EP6-MAH	40	86	162	2.2
Py-EP7-MAH	41	90	194	2.2

Within experimental error, the data listed in Table 3.1 indicate that the seven EPX-MAH samples had similar MWDs.

3.5.2 Determination of SAH content

A calibration curve was generated by preparing films with an EP copolymer, having the same ethylene and propylene content (50 mol%) as the EPX-MAH samples, and different molar ratios of succinic anhydride and characterizing the SAH content of the films by FTIR. The films were cast from ~ 0.5 mL THF solutions containing ~ 0.1 g of non-grafted EP copolymer to which different SAH amounts ranging from 2.2 − 6.0 mg were added from a 24.5 g/L SAH stock solution in THF stored in a 10 mL vial. The viscous mixture was stirred with a small stirrer for 24 hours before use. The mixture was smeared on an FTIR NaCl plate and left to dry with a gentle flow of nitrogen through an 18 Gauge syringe tube. The FTIR spectrum of the film was acquired. It was corrected for background from the FTIR cell to yield an FTIR spectrum such as the one shown in Figure 3.1. The two peaks of interest located at 1462 cm^{-1} and 1785 cm^{-1} represent the bending modes of the methyl group of the propylene units of the EP copolymer and the stretching mode of the SAH carbonyls, respectively.

Several procedures were applied to analyze the FTIR absorption spectra by generating calibration curves from the ratio of the peak intensities at 1462 cm^{-1} and 1785 cm^{-1}. The absorbances were estimated by processing the FTIR spectra through the following mathematical treatments. The calibration curve shown in Figure 3.4A with a slope of 1.68 (±0.08) $\times 10^{-3}$ g.μmol^{-1} was obtained by taking the ratio of the area of the peak at 1785 cm^{-1} over the area of the peak at 1462 cm^{-1} and plotting this ratio as a function of the SAH content (λ_{SAH}) of the mixture expressed in μmol.g^{-1}. The peak areas were then recalculated by defining a baseline that

would bridge the points where the absorption peaks appeared to flatten out on each side of the peak (see geometrical construction in Figure 3.1). This procedure resulted in the calibration curve shown in Figure 3.4B with a slope of 1.43 ($\pm$0.06) $\times$ 10^{-3} g.μmol^{-1}. Taking the ratio of the peak heights yielded the calibration curve shown in Figure 3.4C with a slope of 1.6 ($\pm$0.1) $\times$ 10^{-3} g.μmol^{-1}. Refining the baseline further according to the geometrical construction shown in Figure 3.1 yielded a new set of peak height ratios that resulted in the calibration curve shown in Figure 3.4D with a slope of 1.6 ($\pm$0.1) $\times$ 10^{-3} g.μmol^{-1}. The equations used to determine the peak areas or peak heights for the calibration curves shown in Figures 3.4A-D are listed in the Appendix A. Inspection of Figures 3.4A-D indicates that all procedures used to generate the calibration curves result in a straight line that passes through the origin. The slope (Figures 3.4A-D) of this straight line was used to estimate the SAH content of an unknown maleated EP copolymer sample, as long as the FTIR spectra were processed according to the procedure corresponding to a given calibration curve.
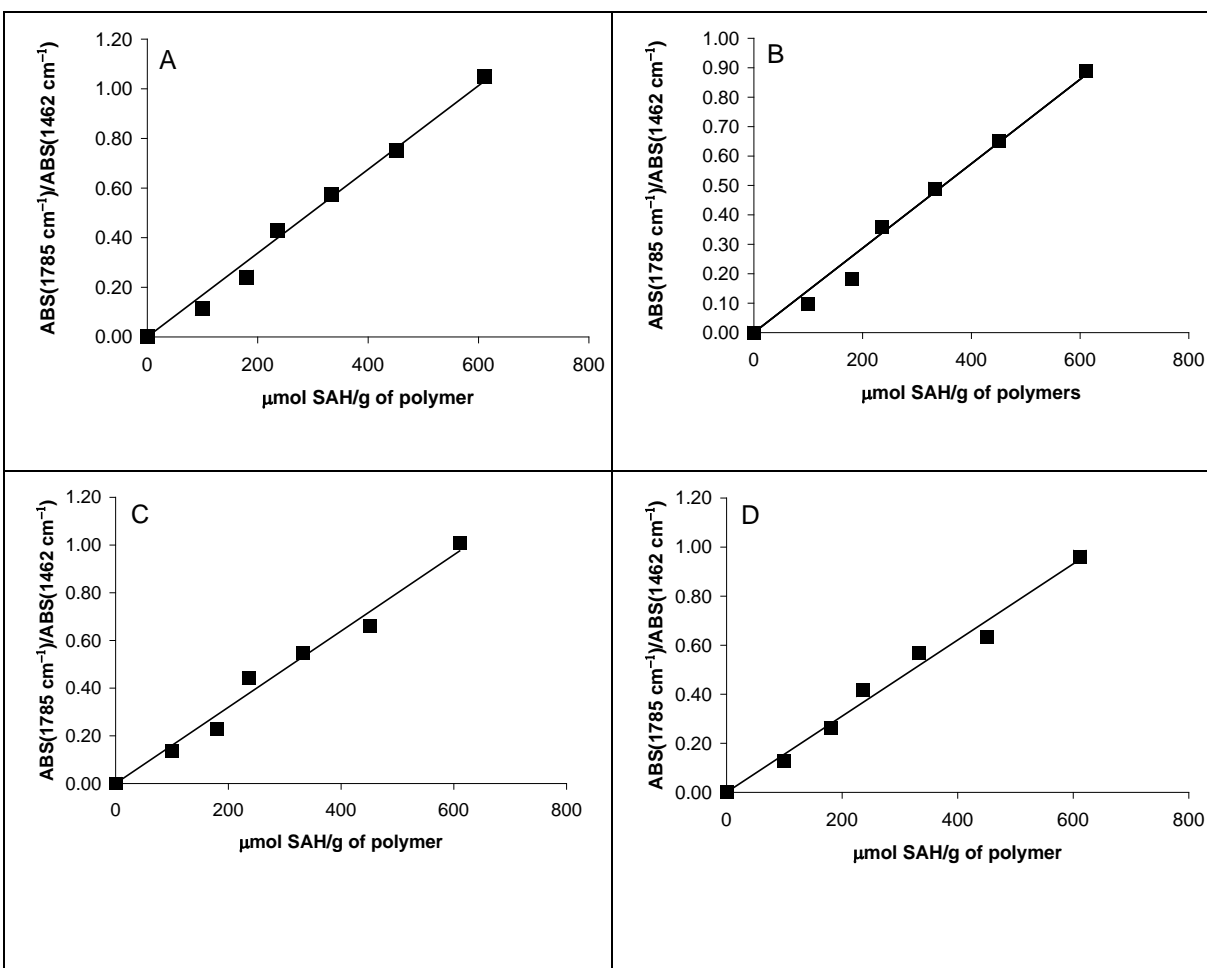
Figure 3.4: Plots of the ratio ABS(1785 cm^{-1})/ABS(1462 cm^{-1}) as a function of SAH content in mixtures of SAH and EP. A) Ratio of the areas under the curve; B) Ratio of the areas under the curve with a base line drawn from each side of the absorption band; C) Ratio of the peak heights; D) Ratio of the peak heights with a base line drawn from each side of the absorption band.

Before acquiring an FTIR spectrum, each EPX-MAH sample (~ 0.5 g) was dissolved in 50 mL of anhydrous dodecane and heated to 130 °C, as determined from a thermometer placed in the oil bath, under nitrogen for 10 h to return the hydrolyzed SAH pendants to their anhydride form. A Dean Stark apparatus and a condenser were installed on the flask. After the EPX-MAH

samples had been converted to their original form, the EPX-MAH solutions were precipitated once from dodecane into acetone. The precipitate was stored in a glass bottle which was placed in a vacuum oven at 120 °C for 5 hours to remove residual traces of solvent and ensure that moisture in the air would not hydrolyze the SAH units. Then, 1 mL of THF was added into the vial which was shaken until a slightly viscous solution was obtained. With the help of a spatula, the EPX-MAH sample was smeared on an FTIR cell and left to dry with a gentle flow of nitrogen from an 18 Gauge needle. Then, the FTIR measurement was conducted.

The SAH content (λ_{SAH}) of the EPX-MAH samples determined according to the calibration curves shown in Figures 3.4A-D are listed in Table 3.2. The FTIR spectra of the seven EPX-MAH samples are shown in Figure 3.5. The film thickness of the EPX-MAH samples was adjusted to ensure that the FTIR absorbance would always be lower than 1.0 and remain within the linear range of the FTIR spectrophotometer detector. The absorption spectra showed a strong peak at 1785 cm^{-1} and no residual absorption at 1710 cm^{-1}, indicating that no hydrolyzed SAH remained in the sample. The SAH content determined with the four calibration curves yielded consistent λ_{SAH} values which were averaged in the last column of Table 3.2.
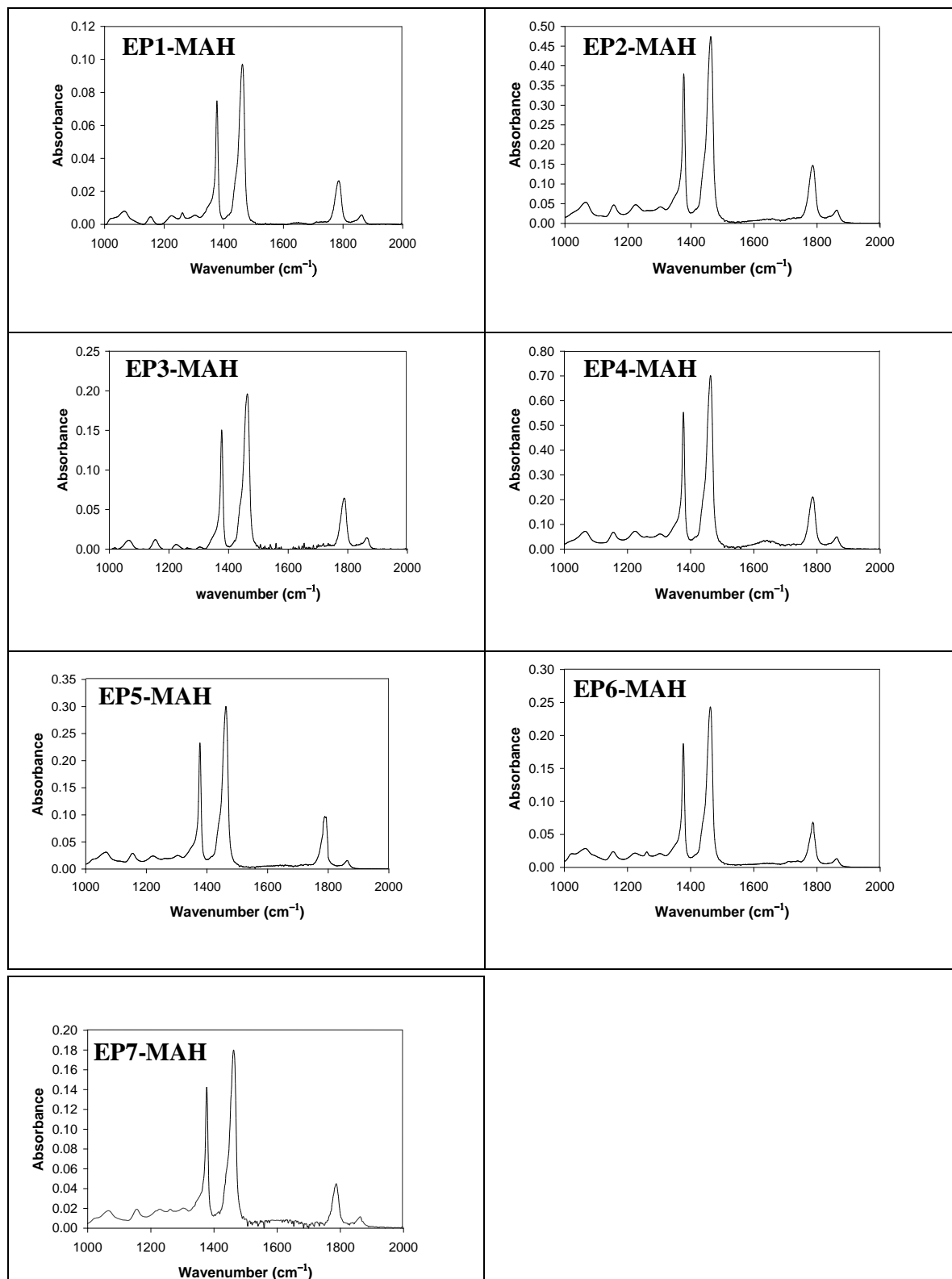
Figure 3.5: FTIR spectra for the EPX-MAH samples.

Table 3.2: SAH content (λ_{SAH}) of the EPX-MAH samples measured with each of the calibration curves shown in Figures 3.4 A-D.

Samples	λ_{SAH} (μmol.g^{-1}) Figure 3.7A	λ_{SAH} (μmol.g^{-1}) Figure 3.7B	λ_{SAH} (μmol.g^{-1}) Figure 3.7C	λ_{SAH} (μmol.g^{-1}) Figure 3.7D	$<\lambda_{SAH}>$ (μmol.g^{-1})
EP1-MAH	168	184	172	170	174 ± 7
EP2-MAH	192	199	194	206	198 ± 6
EP3-MAH	195	196	206	207	201 ± 7
EP4-MAH	183	197	186	209	194 ± 12
EP5-MAH	183	187	202	199	193 ± 9
EP6-MAH	157	183	177	169	171 ± 11
EP7-MAH	151	174	156	153	158 ± 11

3.5.3 Determination of the pyrene content by UV-Vis absorption.

The EPX-MAH samples were labeled with 1-pyrenemethylamine according to the procedure described in the experimental section. The pyrene-labeled EPX-MAH samples (Py-EPX-MAH) were dissolved in tetrahydrofuran (THF) and an absorption spectrum was acquired in triplicate. The spectra obtained for the Py-EPX-MAH samples are shown in Figure 3.6. They exhibit the characteristic absorbance of pyrene with a strong peak at 344 nm that was used to determine the pyrene content of the sample (λ_{Py} expressed in μmol.g^{-1}). The absorption spectra were baseline-corrected and the absorption at 344 nm was divided by the molar absorption coefficient of a model compound, namely 1-pyrenesuccinimide (ε[344 nm, in THF] = 44,500 cm^{-1}.M^{-1}) which was prepared by Jamie Yip, a fellow graduate student in the Duhamel laboratory.

36
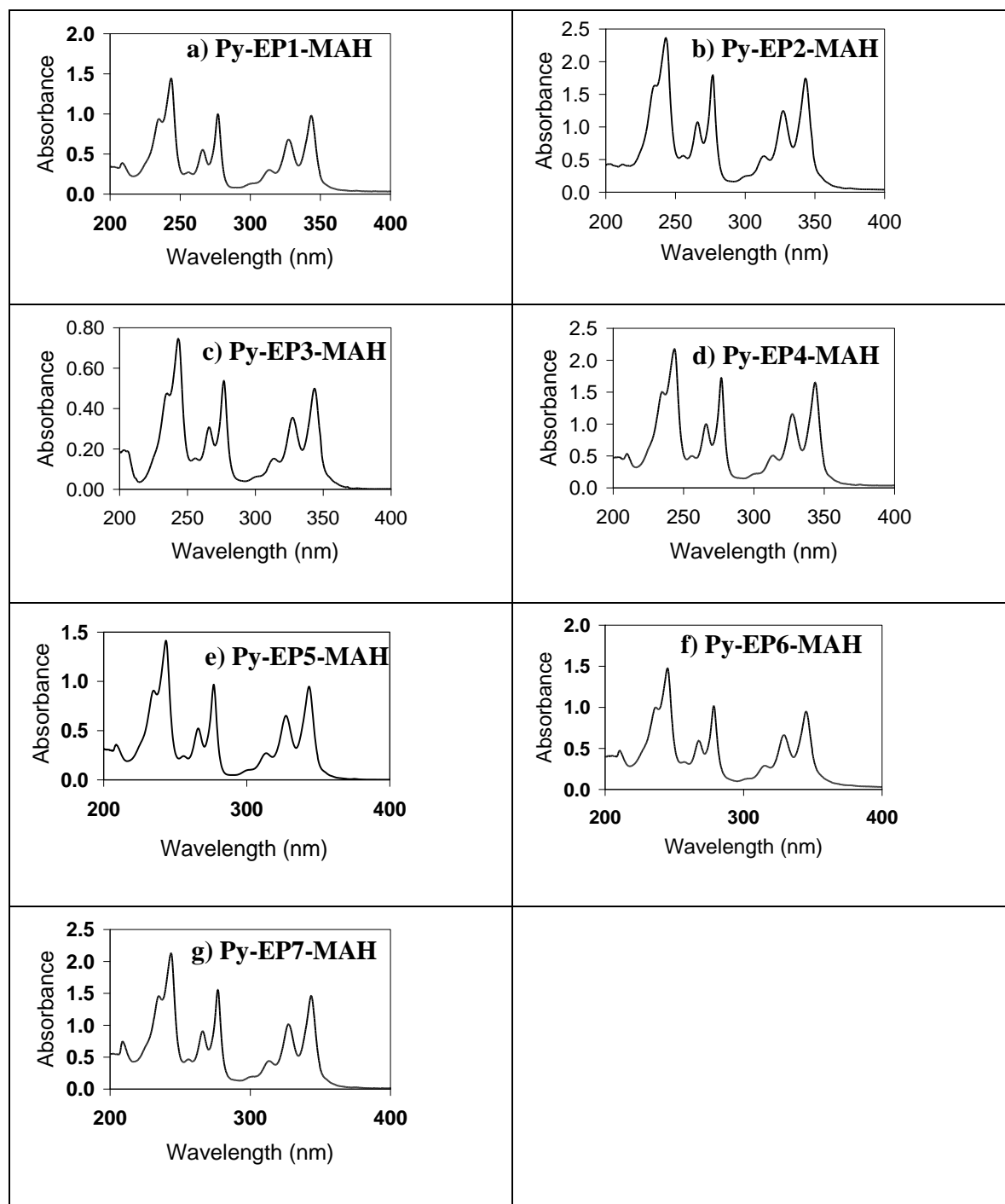
Figure 3.6: UV-Vis absorption spectra of the Py-EPX-MAH samples. The concentrations of the solutions in THF were a) 0.127 g.L^{-1}; b) 0.197 g.L^{-1}; c) 0.075 g.L^{-1}; d) 0.193 g.L^{-1}; e) 0.118 g.L^{-1}; f) 0.131 g.L^{-1}; g) 0.185 g.L^{-1} for Py-EPX-MAH with x=1-7.

The λ_{Py} values obtained for all the pyrene-labeled polymers are listed in Table 3.3. In most cases, a reasonably good agreement is observed between the SAH content obtained by FTIR absorption measurement and the pyrene content obtained by UV-Vis absorption which suggests that the labeling of the SAH pendants by PMA was complete.

Table 3.3: Summary of the pyrene content and SAH content of the samples.

Samples	SAH content (λ_{SAH} in µmol.g^{-1})	Pyrene Content (λ_{Py} in µmol.g^{-1})
EP1-MAH	174 ±7	161 ± 2
EP2-MAH	198 ± 6	194 ± 3
EP3-MAH	201 ± 7	178 ± 6
EP4-MAH	194 ± 12	211 ± 2
EP5-MAH	193 ± 9	191 ± 4
EP6-MAH	171 ± 11	162 ± 3
EP7-MAH	158 ± 11	165 ± 5

3.5.4 Characterization of the level of pyrene clustering in the Py-EPX-MAH samples.

Fluorescence measurements were carried out in tetrahydrofuran (THF) for the Py-EPX-MAH samples labeled with pyrene. To avoid artifacts due to the inner filter effect,[14] the UV-Vis absorbance of the solution for the fluorescence experiments was kept below 0.1. The fluorescence decays for the seven samples are shown in Figure 3.7. According to the modified Birks scheme shown in Figure 3.3, excimer decays typically show a rise time when the excimer is formed via the diffusive encounters between two pyrenes. Most excimer decays showed a rise

time, but in the case of the Py-EP3-MAH and Py-EP6-MAH samples, a spike is clearly observed at the early times. Such a spike has been observed when pyrene aggregates are present in solution.[15]
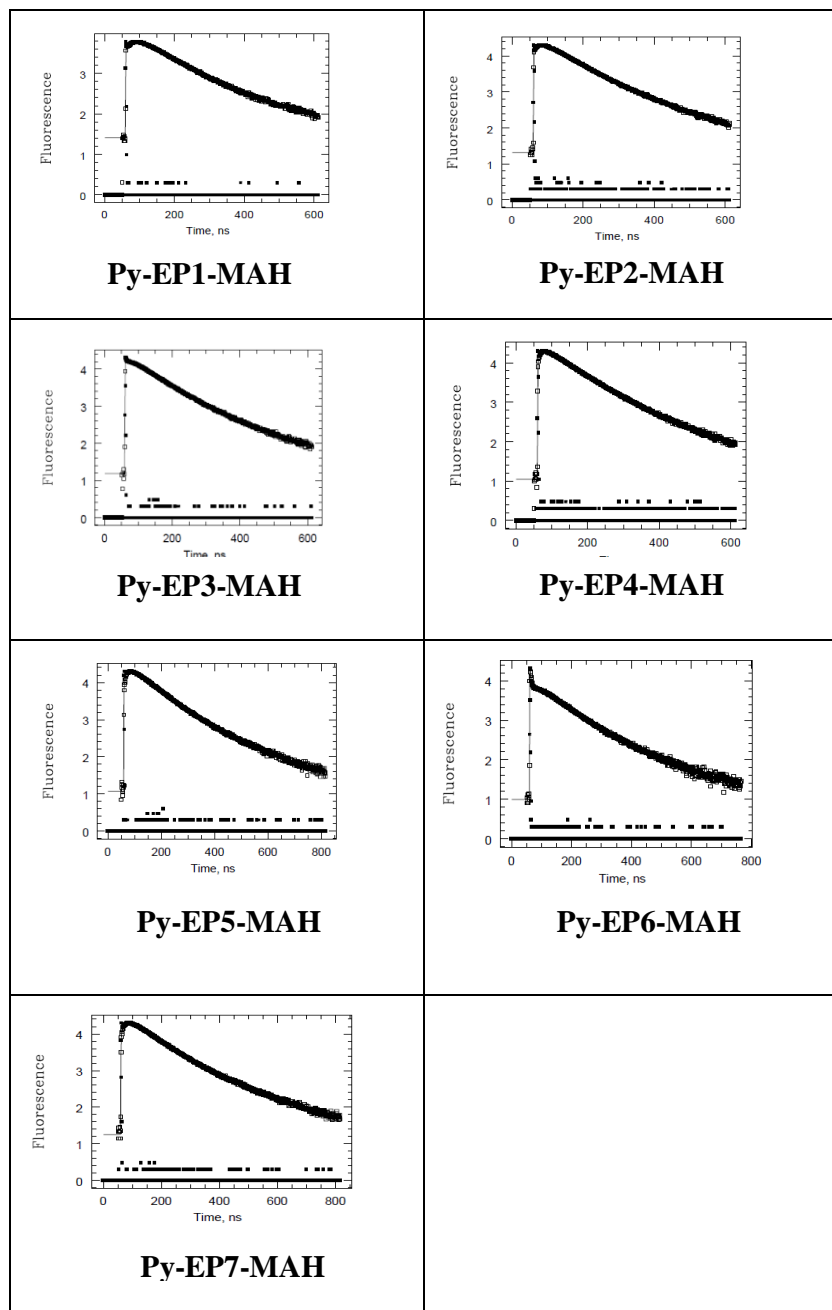
Figure 3.7: Excimer fluorescence decays of the pyrene-labeled samples. $\lambda_{ex} = 344$ nm and $\lambda_{em} = 510$ nm.

The fluorescence decays shown in Figure 3.7 were fitted with a sum of 3 or 4 exponentials according to Equation 3.1 where $N = 3$ or 4.

$$[E^*]_{(t)} = \sum_{i=1}^{N} A_i \exp(-t/\tau_i) \qquad (3.1)$$

Positive pre-exponential factors indicate a decay of the excimer signal whereas negative pre-exponential factors reflect an increase in the excimer signal, i.e. the risetime observed in the fluorescence decays. If no pyrene aggregate is present, the excimer does not exist at time $t = 0$, which implies that the sum $\sum_{i=1}^{N} A_i$ equals zero according to Equation 3.1. Taking the sum of the negative pre-exponential factors (A_-) and dividing it by the sum of the positive pre-exponential factors (A_+) yields the A_-/A_+ ratio which equals -1.0 if $\sum_{i=1}^{N} A_i = 0$. If pyrene aggregates exist in solution, then $\sum_{i=1}^{N} A_i \neq 0$ and the A_-/A_+ ratio takes a value which is more positive than -1.0, i.e. a smaller absolute value. Thus the closer to -1.0 the A_-/A_+ ratio is, the fewer ground-state pyrene aggregates are present in solution. The A_-/A_+ ratios were determined for all the samples and they are listed in Table 3.4. The A_-/A_+ ratios most different from -1.0 are those of Py-EP3-MAH and Py-EP6-MAH, which were suspected to have a larger extent of ground-state pyrene aggregation based on the spike observed at the early times in their fluorescence decays (see Figure 3.7).

Another measure of the presence of ground-state pyrene aggregates was obtained from the P_A value, which is the ratio of the absorbance maximum at 344 nm over the absorbance of the first trough next to the maximum (see Figure 3.2). Broadening of the absorption bands has been

observed as a result of pyrene aggregation.[11] The closer to 3 the P_A value is, the fewer ground-state pyrene aggregates are expected to be present in solution. Using the spectra shown in Figure 3.6, the P_A values were calculated and they are listed in Table 3.4. Here again, the lowest P_A value is that of the Py-EP3-MAH and Py-EP6-MAH samples, suggesting that these samples contain a larger amount of ground-state pyrene aggregates as inferred from the A_-/A_+ ratios.

The data listed in Table 3.4 imply that samples Py-EP3-MAH and Py-EP6-MAH exhibit the largest amount of ground-state pyrene aggregates, suggesting that the SAH pendants are distributed in a clustered manner along this backbone. The SAH groups might be slightly more clustered for sample Py-EP2-MAH than for samples Py-EP1-MAH, Py-EP4-MAH, EP5-MAH, and EP7-MAH, which are similar in terms of the distribution of SAH groups and show the most random distribution of pyrene pendants along the polymer backbone.

Table 3.4: P_A and A_-/A_+ ratios for the pyrene labeled samples.

Pyrene-labeled sample	P_A	A_-/A_+
Py-EP1-MAH	2.79 ± 0.01	-0.79
Py-EP2-MAH	2.64 ± 0.01	-0.63
Py-EP3-MAH	2.35 ± 0.03	-0.25
Py-EP4-MAH	2.83 ± 0.01	-0.80
Py-EP5-MAH	2.93 ± 0.02	-0.84
Py-EP6-MAH	2.42 ± 0.03	-0.21
Py-EP7-MAH	2.89 ± 0.02	-0.84

Since the non-labeled EPX-MAH samples exhibited some residual short-lived fluorescence, it became important to assess whether the spikes observed at the early times in the excimer decays of Py-EP3-MAH and Py-EP6-MAH were not due to the polymer itself. Consequently, dilute solutions of all EPX-MAH samples were prepared at the polymer concentrations used to acquire the excimer fluorescence decays shown in Figure 3.7. The fluorescence decays of these solutions were obtained and are shown in Figure 3.8. Since the emission is weak, the decays showed a substantial amount of background noise. The ratio of the background over that of the peak set to equal 10,000 counts (BG/Peak) provided a measure of the importance of the fluorescence emitted by the naked EPX-MAH samples, and is in essence a measure of the fluorescence quantum yield of the naked EPX-MAH samples. The BG/peak ratios have been listed in Figure 3.8. According to Figure 3.8, EP3-MAH and EP4-MAH yield similar BG/Peak ratios; yet a spike is observed in the excimer decay of Py-EP3-MAH and not in the excimer decay of Py-EP4-MAH. Also, the BG/peak ratio of EP6-MAH is close to that of EP1-MAH and EP7-MAH where as a spike is only detected in the fluorescence decay of Py-EP6-MAH. Since all EPX-MAH samples considered appear to have similar fluorescence quantum yields based on their BG/Peak ratios, these results confirm that the spike detected in the excimer fluorescence decays of Py-EP3-MAH and Py-EP6-MAH is due to interactions between pyrene pendants and not residual emission from the polymer.
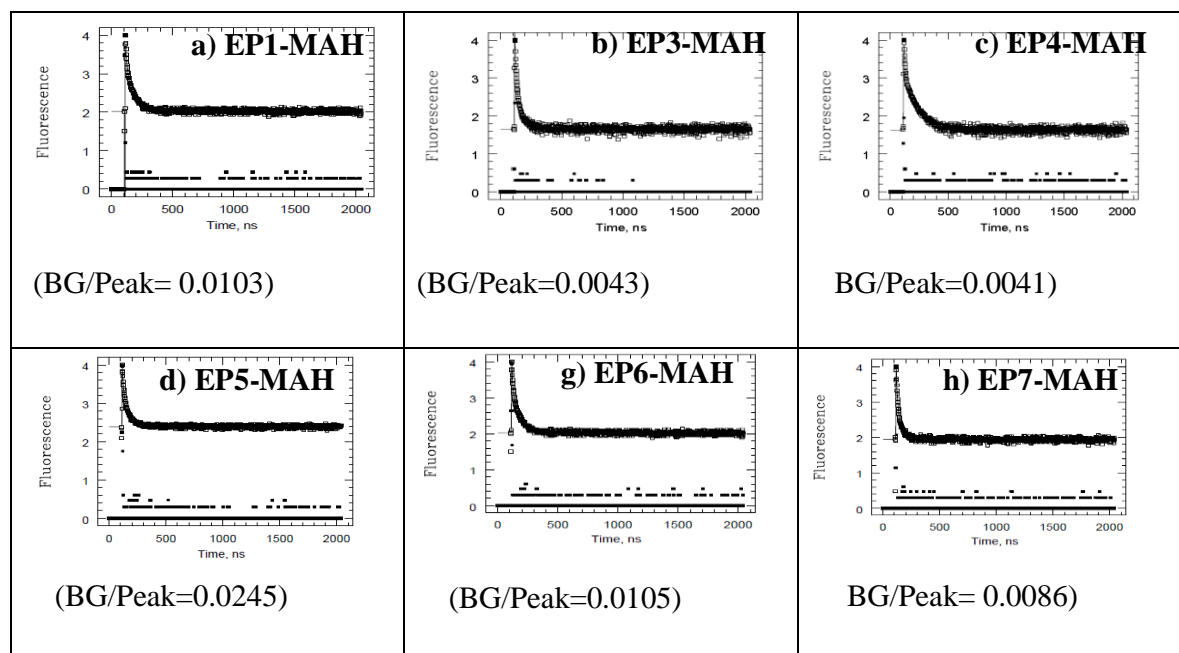
Figure 3.8: Fluorescence decays of EPX-MAH samples. $\lambda_{ex} =344$ nm and $\lambda_{em}= 510$ nm.

Polymer concentration in THF were: a) 12 mg.L^{-1}; b) 11 mg.L^{-1}; c) 13 mg.L^{-1}; d) 14 mg.L^{-1}; e)

15 mg.L^{-1}; f) 13 mg.L^{-1} for EPX-MAH with X=1-6.

CHAPTER 4: EFFECT OF SAH CLUSTERING ON THE SOLUTION BEHAVIOR OF MODIFIED EP COPOLYMERS

4.1 Introduction

The purpose of this study was to determine whether the clustering of SAH pendants along a maleated EP copolymer would have any effect on the solution properties of the polymer, most importantly on the solution properties relevant to the oil-additive industry. The seven EPX-MAH samples that were supplied by DSM and whose molecular weight distribution, SAH content, and level of SAH clustering were characterized in Chapter 3 constituted an ideal group of samples to reach that goal. The ability of the modified EPX-MAH samples to associate in solution via their succinimide pendants was probed by fluorescence in solvents of different polarities, namely tetrahydrofuran and hexane with dielectric constants equal to 7.6 and 1.89, respectively. Whereas the entire polymers are fully soluble in THF, their succinimide pendants are not soluble in hexane. Consequently, intra- and interpolymeric associations occur in hexane.

Viscosity measurements were conducted to characterize the influence of clustering of the SAH pendants on interpolymeric association in hexane. Finally, the adsorption of the modified EPX-MAH samples onto carbon black particles (CBPs) was characterized by constructing Langmuir isotherms. Analysis of the Langmuir isotherms provided information on the influence of SAH clustering on the adsorption phenomenon. The fluorescence, viscosity, and adsorption experiments are described in detail in the following sections.

In the present work, measurements were conducted to investigate the solution properties of five polymer samples in hexane and in THF. The selection of the five samples was based on the following rational. The results listed in Tables 3.1 and 3.3 indicate that Py-EP3-MAH and Py-EP5-MAH on the one hand and Py-EP6-MAH and Py-EP7-MAH on the other hand have similar pyrene contents and molecular weight distribution, the main difference between those samples

being the level of pyrene clustering. Sample Py-EP4-MAH with the highest pyrene content was also studied to investigate the effect of pyrene content. Consequently, samples EPX-MAH with X= 3-7 were selected to study their solution properties.

4.2 Fluorescence techniques

Since pyrene is covalently attached onto the SAH pendants, the presence of oligoMAH and SAH clusters along the polymer chain creates pyrene domains which promote the formation of pyrene ground-state dimers, even in a solvent which does not promote pyrene-pyrene associations such as THF. The presence of pyrene ground-state dimers can be established by carrying out a variety of experiments that include UV absorption or time-resolved fluorescence measurements. These experiments were described in Chapter 3. Pyrene aggregation is also expected to induce a spectral shift between the excitation spectra of Py-EPX-MAH in hexane acquired with an emission wavelength fixed at either 375 nm (for the pyrene monomer) or 500 nm (for the pyrene excimer).[1,2] This spectral shift is illustrated in Figure 4.1 A-J for the Py-EPX-MAH samples with X=3-7. The spectral shift is usually strongly reduced in THF, indicating that much less pyrene ground-state dimers are formed in THF, as shown in Figure 4.1 A-E. The much stronger spectral shifts detected in Figures 4.1 F-J demonstrates that the Py-EPX-MAH samples undergo intra- and interpolymeric association in hexane via their polar succinimide pendants. This process, which is strongly reduced in more polar THF, induces the formation of pyrene aggregates in hexane whose presence in clearly demonstrated from the shifts displayed in Figure 4.1 F-J.

Information on how the solvent polarity alters the influence of SAH clustering on the association of modified EP-MAH polymers can be obtained by acquiring an emission spectrum

and monitoring the ratio of the fluorescence intensity over that of the monomer, i.e. the I_E/I_M ratio.[2] Regardless of how the excimer is being formed, a change in the I_E/I_M ratio usually indicates a transition in the process of excimer formation (see Figure 3.3). Figures 4.2 A-E in THF and F-J in hexane show the emission spectra of the samples Py-EPX-MAH with X=3-7 with the pyrene monomer exhibiting sharp peaks between 370 and 400 nm and the excimer fluorescing as a structureless band centered at 480 nm. The I_E/I_M ratio which gives information on the efficiency of eximer formation was determined for each polymer. In both solvents, Py-EP3-MAH and Py-EP6-MAH yield larger I_E/I_M ratios suggesting that excimer formation is more efficient, in agreements with the more clustered distribution of pyrene pendants expected for these two samples.

Qualitative information about the level of association between the polar moieties in different solvents was also obtained from the P_A and A_-/A_+ ratios.
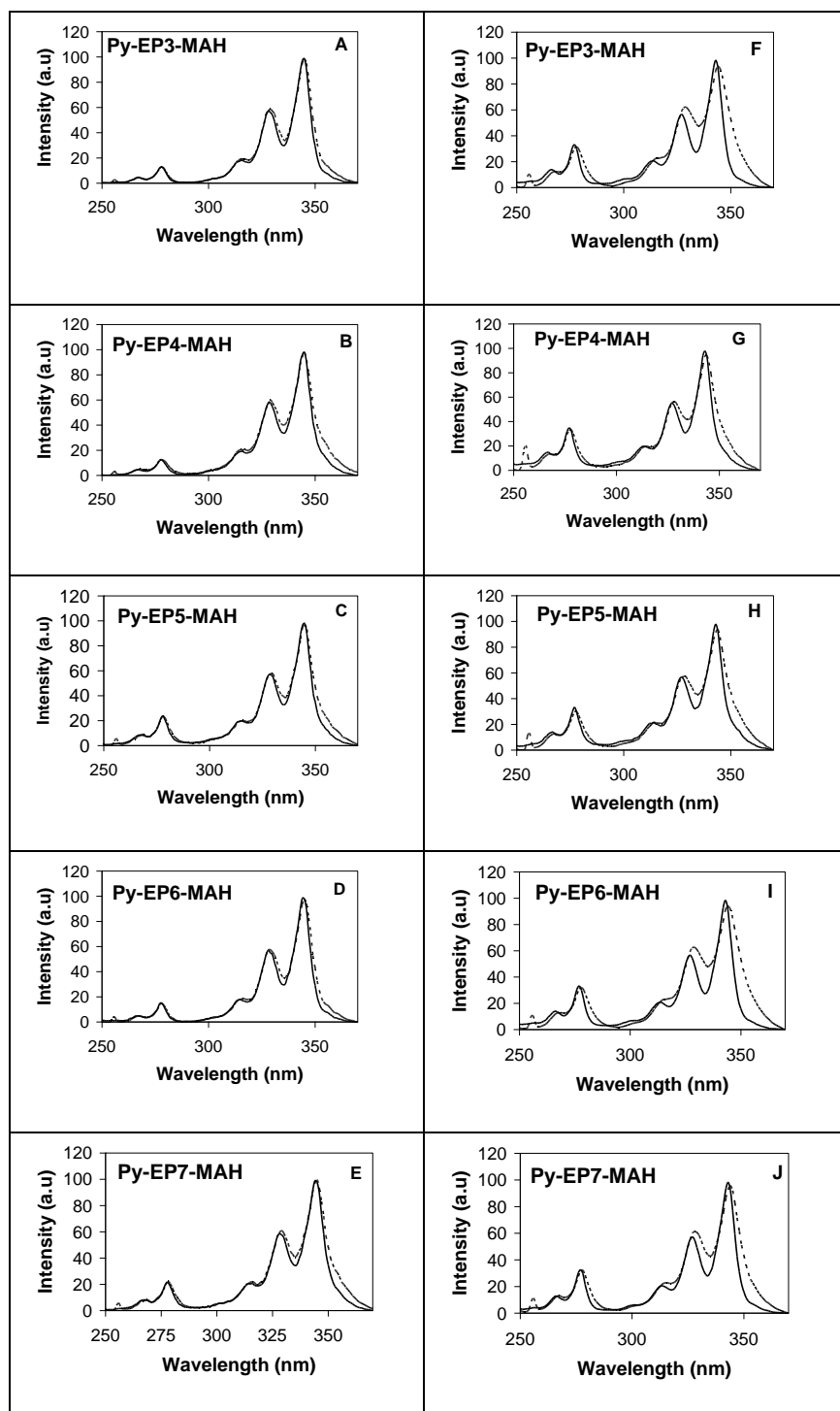
Figure 4.1: Excitation spectra using an emission wavelength of 375 and 510 nm for the
pyrene monomer and excimer, respectively. A-E in THF; F-G in hexane for samples Py-
EPX-MAH with X=3-7.
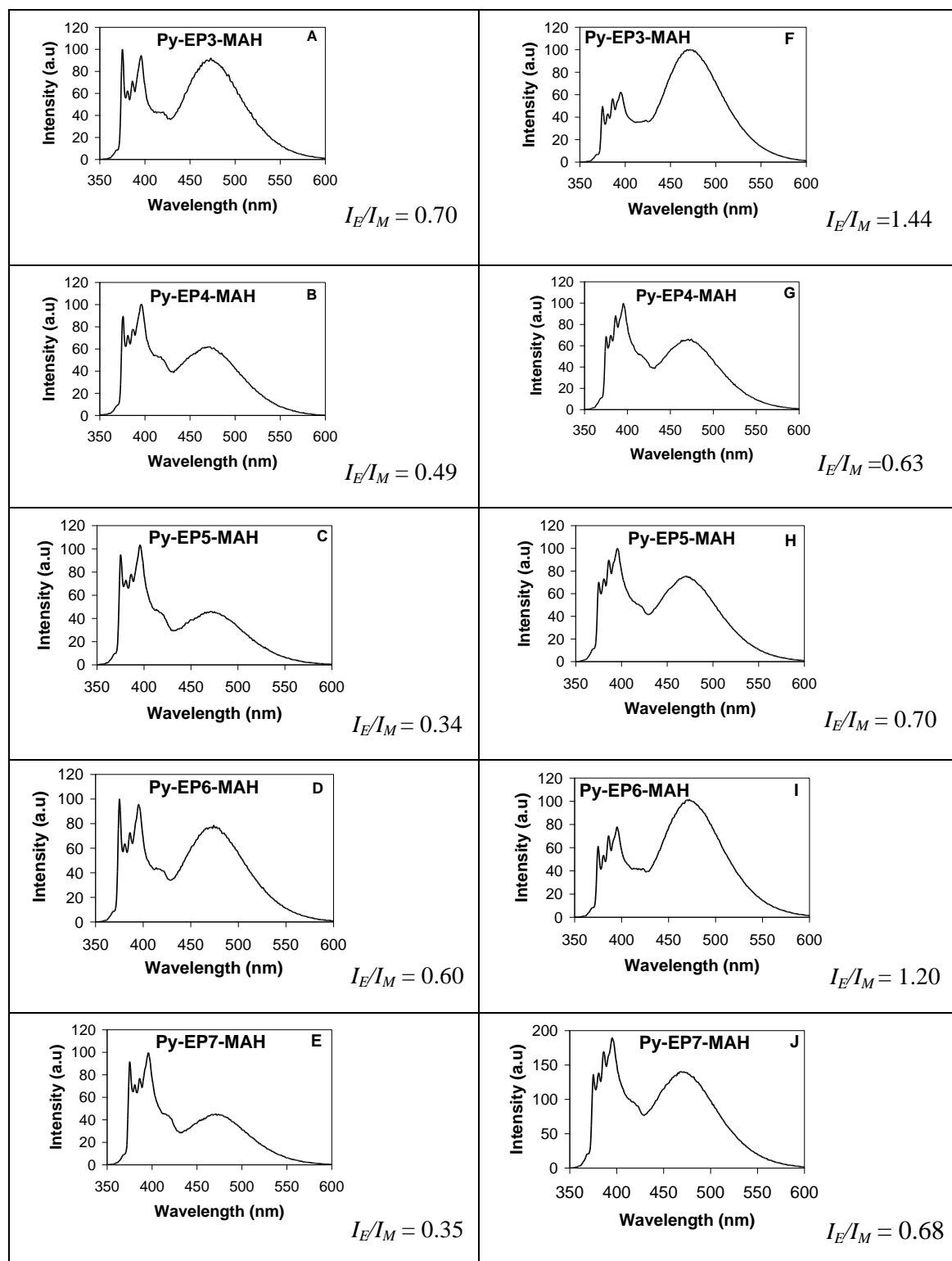
Figure 4.2: Fluorescence emission spectra of Py-EPX-MAH samples A-E and F-J in

THF and hexane, respectively. λ_{ex} 344 nm. Polymer concentrations from 11 to 13 mg.L^{-1}.

49

The P_A values for the Py-EPX-MAH samples in hexane were all smaller than 2.2, indicating strong pyrene aggregation. All P_A values obtained in hexane were lower than in THF. The lowest P_A values were reached with Py-EP3-MAH and Py-EP6-MAH, indicating the stronger ability of these samples to self-associate in hexane. This is a result of the associations taking place in hexane between the polar succinimide pendants resulting from the labeling of the EP-MAH samples with 1-pyrenemethylamine. Py-EP3-MAH and Py-EP6-MAH yielded the lowest P_A values in hexane, indicating that dipolar associations induced by the succinimide moieties are further enhanced if the polar groups are clustered along the backbone. In addition, the A_-/A_+ ratios were determined by analysis of the excimer fluorescence decays of the Py-EPX-MAH solutions in hexane. The A_-/A_+ ratios were more positive in hexane than in THF (cf. Table 3.4), reflecting that pyrene aggregation is more efficient in hexane than in THF. The A_-/A_+ ratio most different from -1.0 is that of the pyrene-labeled Py-EP3-MAH and EP6-MAH samples which were determined to have a clustered distribution of the pyrene pendants along the backbone (Figure 4.3)
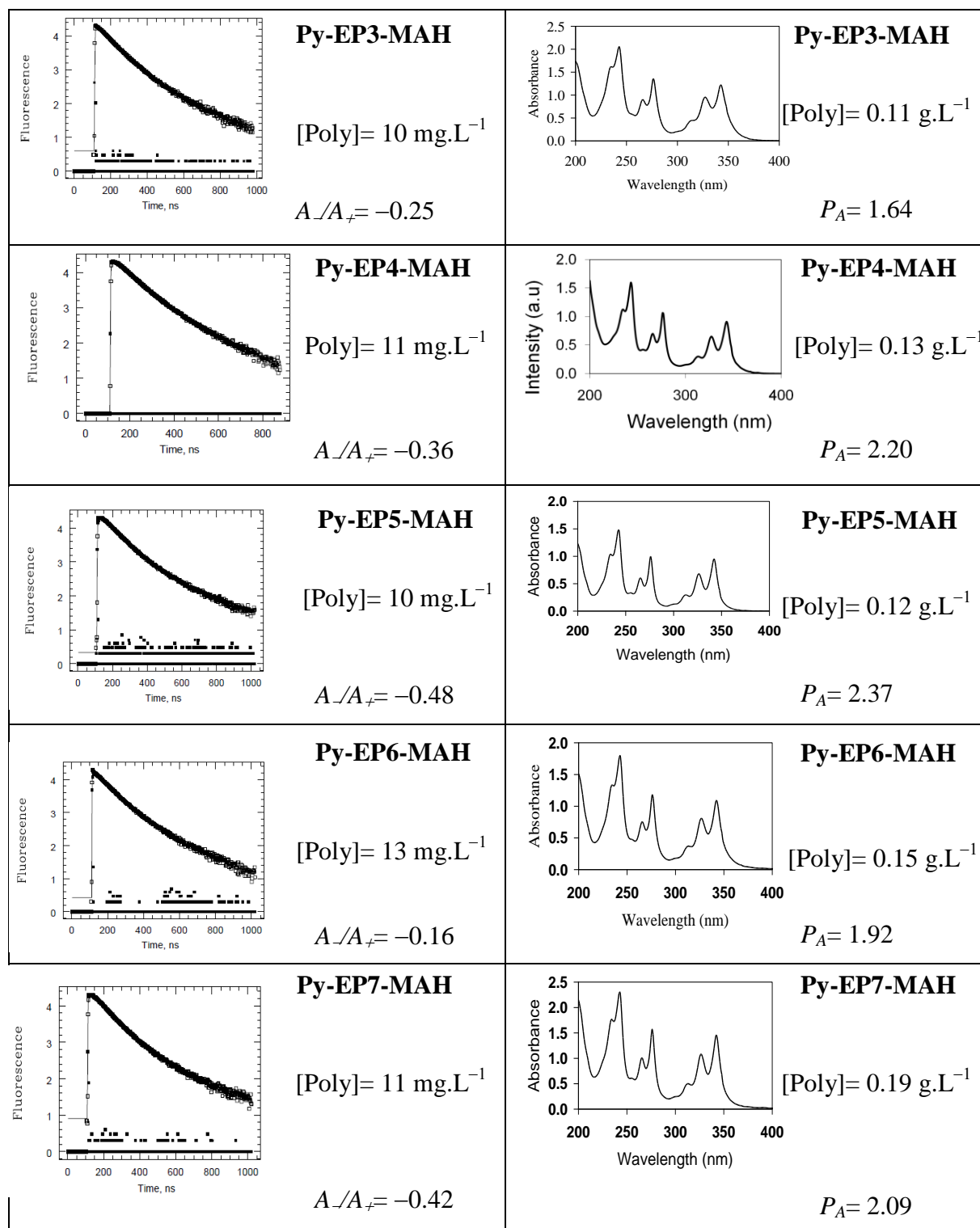
Figure 4.3: P_A and A_-/A_+ ratios for the pyrene labeled samples in hexane. Polymer concentrations ranging from 11 to 13 mg.L^{-1}.

4.3 Viscosity of the Py-EPX-MAH solutions.

In 2005, a study conducted by Zhang et al.[3] showed that SAH clustering affects the rheological properties of modified EP copolymers in solution. As shown in Figure 4.4 where the viscosity of the polymer solution was plotted as a function of polymer concentration, the Py-EPX-MAH samples exhibited a much steeper viscosity increase with polymer concentration in hexane than in THF. This behavior is attributed to the formation of interpolymeric aggregates in hexane that hinder the flow of the solution and increase the viscosity. The formation of interpolymeric aggregates in hexane is induced by dipolar interactions between the succinimide pendants. As shown in Figure 4.1 by fluorescence, these polar interactions are much reduced in polar THF which results in a significant decrease in solution viscosity at high polymer concentration. Interestingly, whereas all viscosity profiles overlapped each other in THF, major differences were observed between them in hexane. In particular, the viscosity profiles obtained for samples Py-EP3-MAH and Py-EP6-MAH exhibited a much steeper increase with polymer concentration than those obtained with Py-EP4-MAH, Py-EP5-MAH, and Py-EP7-MAH. Samples Py-EP3-MAH and Py-EP6-MAH also happen to be those whose clustered SAH distribution along the chain was shown to induce strong associations between the pyrene pendants. The results shown in Figure 4.4 demonstrate the correlation that exists between the level of clustering of the SAH pendants in an EP-MAH sample and the viscosity profile of that polymer solution as a function of polymer concentration. The steeper increase observed for Py-EP3-MAH compared to Py-EP6-MAH might be due to the higher SAH content of the Py-EP3-MAH sample (see Table 3.3).
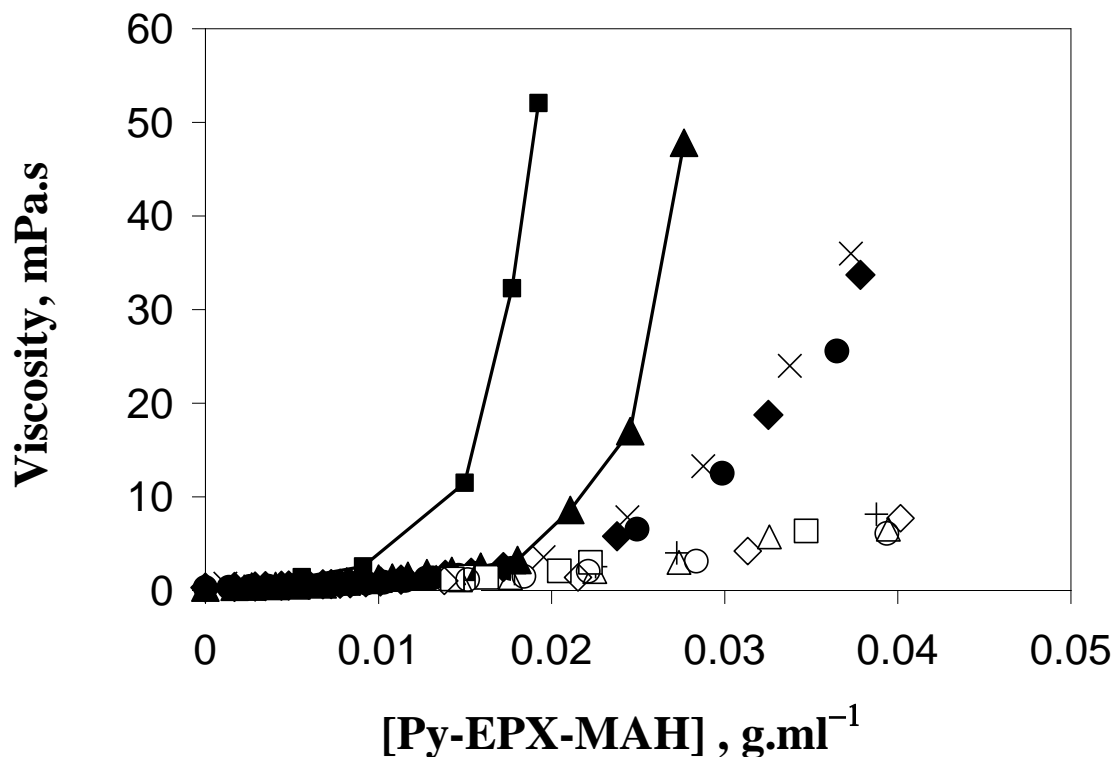
Figure 4.4: Plot of viscosity versus polymer concentration. In hexane: Py-EP3-MAH (■), Py-EP4-MAH (×), Py-EP5-MAH (●), Py- EP6-MAH (▲), Py-EP7-MAH (◆). In THF: Py-EP3-MAH(□), Py-EP4-MAH(+), Py-EP5-MAH (○), Py- EP6-MAH (△), Py-EP7-MAH (◇).

4.4 Binding of NP$_3$D-EPX-MAH on CBPs.

The adsorption of polymers onto solid surfaces has been and continues to be the focus of intense research.[4-10] The adsorption of macromolecules such as the polyisobutylene succinimide (PIBSI) molecules shown in Figure 4.5A onto solid surfaces has been carefully investigated.[5,7,9] However, the adsorption of maleated EP copolymers with amine containing pendants such as *N*-

phenyl-*p*-phenylaminesuccinimide (NP$_3$D-Su Figure 4.5B), a side-group whose structure is often encountered in the patent literature, [11-13] has not been reported in the scientific literature.
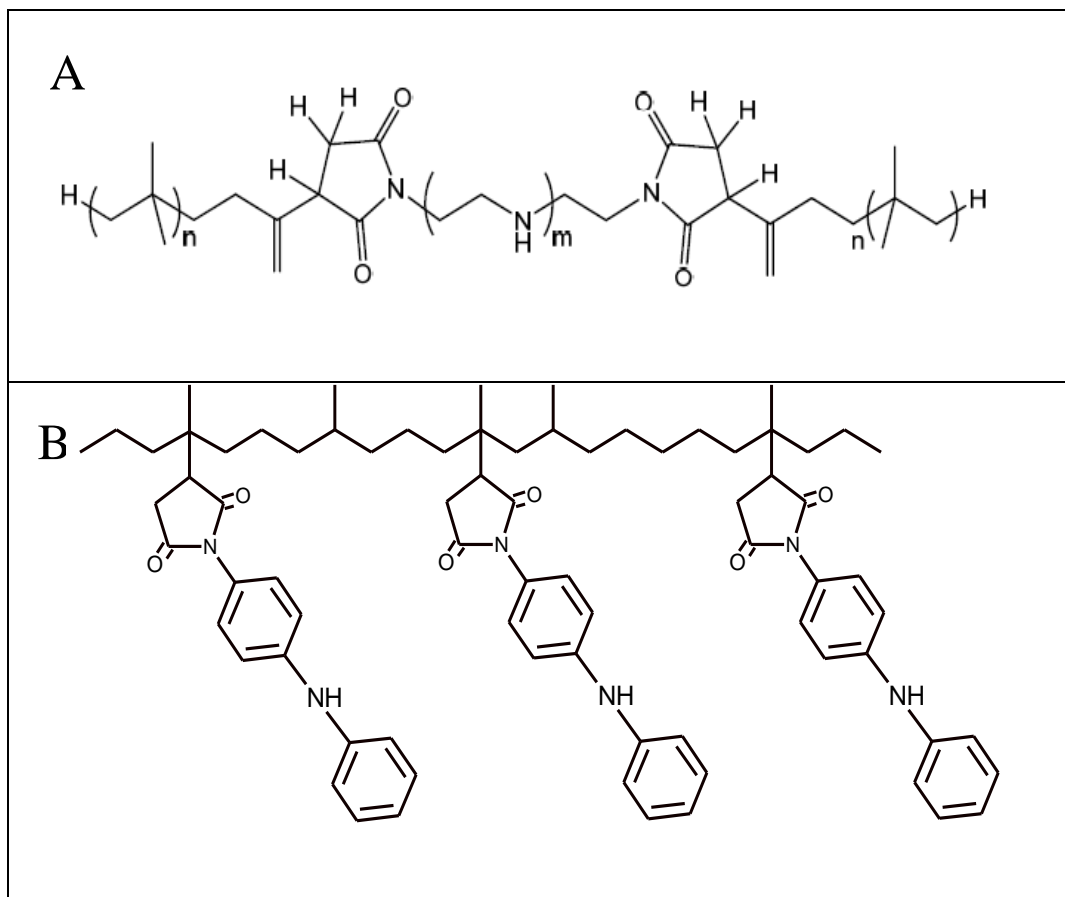
Figure 4.5: Chemical structure of the dispersants A) PIBSI-PETA and B) NP$_3$D-EP-MAH.

This section describes how the level of SAH clustering affects the binding efficiency of the NP$_3$D-EPX-MAH samples onto carbon black particles (CBPs). The adsorption efficiency of the dispersants onto CBPs was determined by constructing the Langmuir isotherms which were then analyzed to yield both the equilibrium constant (K) and the maximum coverage (Γ_{max}).

4.4.1 Adsorption

Several terms are often used to describe the adsorption of molecules onto solid surfaces and their definition is given hereafter. The adsorbate represents the material in the adsorbed state. The substance that is free in solution before adsorption has actually occurred is called the adsorpt or adsorptive (Figure 4.6).[14]
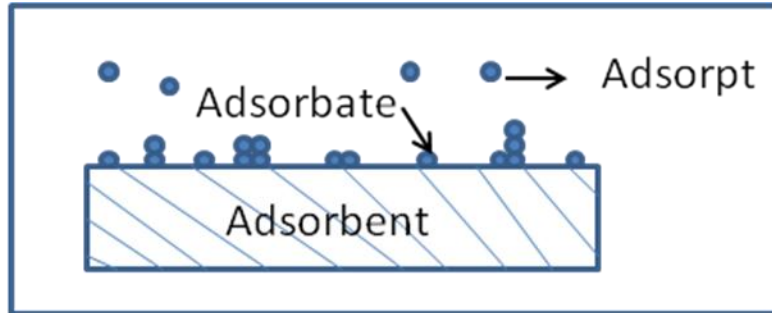
Figure 4.6: Definition of the adsorbent, adsorpt, and adsorbate.[14]

The amount of dispersant that is adsorbed at the interface is described by the adsorption function $\Gamma = f(C_{eq}, T)$ which is determined experimentally. It represents the grams of adsorbate per unit area of adsorbent. The function Γ depends on the temperature (T) and the concentration of adsorpt (C_{eq}). A plot of Γ versus C_{eq} at constant temperature is called an adsorption isotherm. The adsorption function is calculated with Equation 4.1.

$$\Gamma = \frac{(C_0 - C_{eq}) \times V}{m \times A} \tag{4.1}$$

where C_0 represents the initial concentration of the dispersant, C_{eq} indicates the concentration of the dispersant in the supernatant, V is the volume of the solution, m and A are the mass of CBPs

added to the solution and the surface area of the CBPs, respectively. *A* was taken to equal 764 $m^2.g^{-1}$ as found in an earlier report.[5]

The adsorption isotherm was analyzed according to Equation 4.2 which is derived in the Appendix B assuming single adsorption sites. In the case of the NP_3D-EP-MAH samples, it can be assumed that each NP_3D pendant binds a single site onto the CBP surface.

$$\Gamma = \frac{\Gamma_{max} \times K_{eq} \times C_{eq}}{1 + K_{eq} \times C_{eq}} \tag{4.2}$$

4.4.2 Determination of the NP₃D content by UV-Vis absorption

After the EPX-MAH samples were labeled with NP_3D, the NP_3D-EPX-MAH samples were dissolved in tetrahydrofuran (THF) and an absorption spectrum was acquired in triplicate. The spectra obtained for the NP_3D-EPX-MAH samples are shown in Figure 4.7 for X=3-7. They exhibit a strong absorbance peak at 294 nm that was used to determine the NP_3D content of the sample (λ_{NP3D} expressed in $\mu mol.g^{-1}$). The absorption spectra were baseline-corrected and the absorbance at 294 nm was divided by the molar absorbance coefficient of a model compound, namely the succinimide of NP_3D, ($\varepsilon[294 \text{ nm, in THF}] = 20,400 \text{ cm}^{-1}.M^{-1}$).
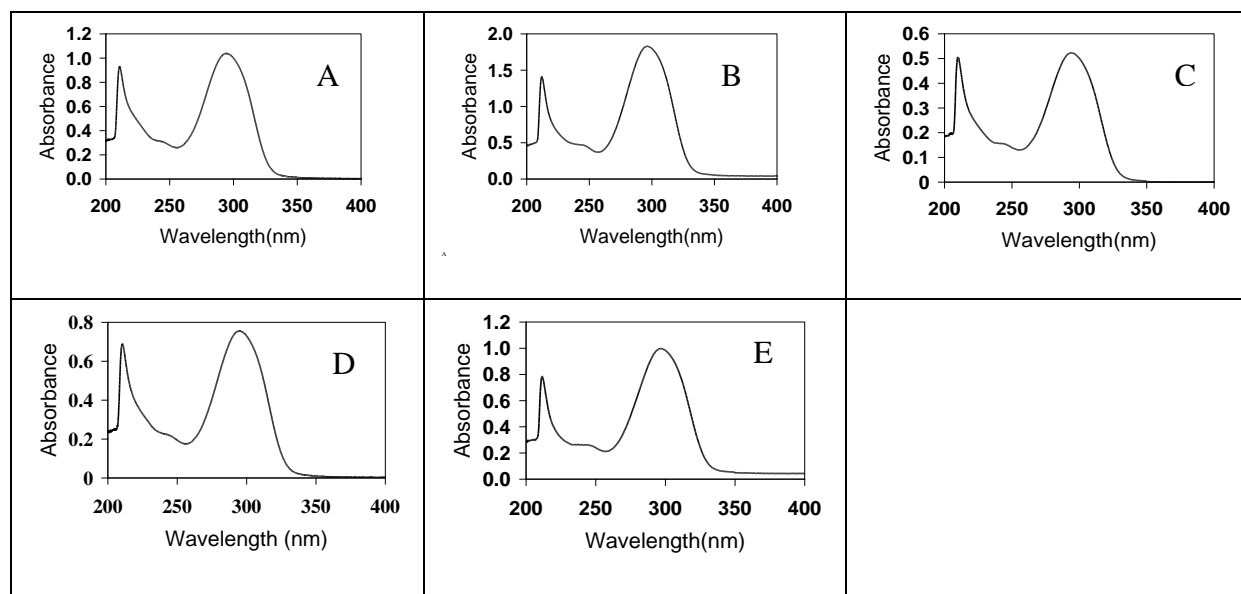
Figure 4.7: Absortion spectra of NP$_3$D-EPX-MAH samples in THF. A) [NP$_3$D-EP3-MAH]= 0.305 g.L^{-1}; B) [NP$_3$D-EP4-MAH]= 0.431 g.L^{-1} ; C) [NP$_3$D-EP5-MAH]=0.125 g.L^{-1} D) [NP$_3$D-EP6-MAH]= 0.218 g.L^{-1}; E) [NP$_3$D-EP7-MAH]= 0.245 g.L^{-1}.

The λ_{NP3D} values obtained for the five NP$_3$D-EPX-MAH (X=3-7) used in the adsorption study are listed in Table 4.1 together with the λ_{Py} values that were obtained in Chapter 3. In all cases, a reasonably good agreement is observed between the pyrene and NP$_3$D content obtained by UV-Vis absorption measurements.

Table 4.1 : Summary of the pyrene content and NP_3D content of the samples.

Samples	NP_3D content (λ_{NP3D} in $\mu mol.g^{-1}$)	Pyrene Content (λ_{Py} in $\mu mol.g^{-1}$)
EP3-MAH	174 ± 10	178 ± 6
EP4-MAH	199 ± 6	211 ± 2
EP5-MAH	201 ± 5	191 ± 4
EP6-MAH	172 ± 4	162 ± 3
EP7-MAH	185 ± 8	165 ± 5

4.4.3 Adsorption isotherms analysis

The adsorption isotherms were constructed according to the following protocol. A solution of 0.09 g of NP_3D-EPX-MAH sample in 65 mL of anhydrous dodecane was prepared and agitated for 72 hours. Dodecane was used instead of hexane for the adsorption experiments as the NP_3D-EPX-MAH samples were found to adsorb onto the Millipore filters used later on in the procedure when working with NP_3D-EPX-MAH solutions in hexane. This complication was avoided by preparing the solutions in dodecane. Masses ranging from 0.01 to 0.4 g of CBPs were added. The samples were agitated in a shaker at 350 rpm for 17 hours at room temperature (25 °C). After equilibrium was reached, the solids were filtered through 0.4 µm amphiphilic Millipore filters. The absorbance at 294 nm of the supernatant was measured to calculate the NP_3D concentration and in turn, the NP_3D-EPX-MAH concentration based on the λ_{NP3D} values listed in Table 4.1. Figure 4.8 shows the adsorption isotherms of the NP_3D-EPX-MAH samples in dodecane together with those obtained for two polyisobutylene dispersants, namely PIB-DETA and PIB-PEHA.[5] These dispersants were obtained from the reaction of two polyisobutylene chains

terminated at one end with one succinic anhydride with diethylene triamine (DETA) and pentaethylene hexamine (PEHA). The profiles of the isotherms obtained for the PIB-based dispersants are of the Langmuir type.[15] Those obtained for the NP$_3$D-EPX-MAH samples are characteristic of multilayer formation.[15] However, the early points of these isotherms obtained with small C_{eq} values (i.e C_{eq} <10 mg/L) represent the formation of a monolayer at the CBP surface and should be well described by a Langmuir isotherm.
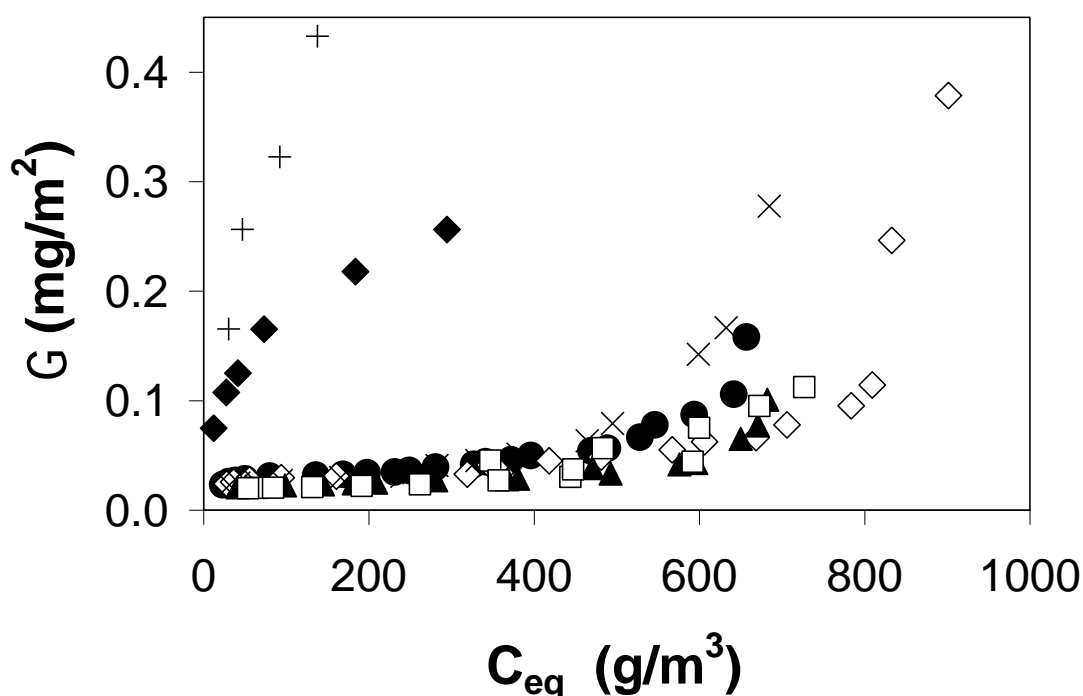
Figure 4.8: Adsorption isotherms of NP$_3$D-EP3-MAH (□), NP$_3$D –EP4 MAH(×), NP$_3$D -EP5-MAH (●), NP$_3$D-EP6-MAH (▲), NP$_3$D -EP7-MAH (◇), in dodecane. PIB-PEHA (◆) and PIB-DETA(+) in hexane.

Figure 4.9 shows the plots of 1/Γ as a function of 1/C_{eq} of the NP$_3$D-EPX-MAH samples. The behavior of NP$_3$D-EP3-MAH and NP$_3$D-EP6-MAH are different from that of the NP$_3$D-EP4-

MAH, NP$_3$D-EP5-MAH, and NP$_3$D-EP7-MAH samples. For $C_{eq} < 10$ mg.L^{-1} the trends shown in Figure 4.9 can be analyzed with Equation 4.2 to yield Γ_{max} (g/m^2) which represents the maximum amount of dispersant that can adsorb onto the CBPs and K (m^3/g) which is the binding equilibrium constant.
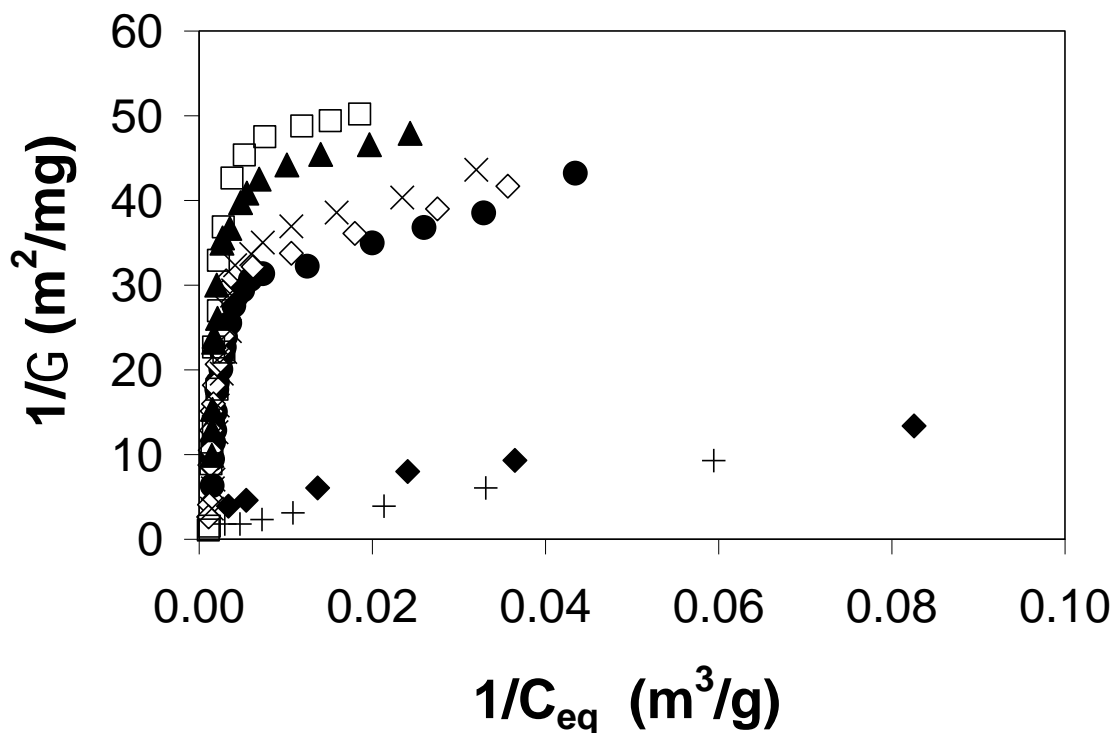
Figure 4.9: Plot of $1/\Gamma$ as a function of $1/C_{eq}$ for NP$_3$D-EP3-MAH (□), NP$_3$D–EP4-MAH (×), NP$_3$D-EP5-MAH (●), NP$_3$D-EP6-MAH (▲), NP$_3$D-EP7-MAH (◇ in dodecane. PIB-PEHA (◆) and PIB-DETA (+) in hexane.

The values of Γ_{max} and K are listed in Table 4.2. Those values reflect the trends observed in Figure 4.9 where three types of binding can be isolated. The samples with clustered SAH pendants, namely NP$_3$D-EP3-MAH and NP$_3$D-EP6-MAH, yield the largest binding constant K,

followed by NP$_3$D-EP4-MAH, NP$_3$D-EP5-MAH, and NP$_3$D-EP7-MAH, and with the samples PIBSI-DETA and PIBSI-PEHA yielding the smallest binding constants. On the other hand, the Γ_{max} values follow an inverse trend, being largest for the PIBSI-based dispersants, followed by the three NP$_3$D-EP-MAH samples having NP$_3$D-Su pendants better distributed along the chain, and with the samples NP$_3$D-EP3-MAH and NP$_3$D-EP6-MAH yielding the lowest Γ_{max} values.

Table 4.2: Comparison of Γ_{max} (g/m^2) and K (m^3/g) of the two dispersants.

Sample	Γ_{max} (g/m^2)	K (m^3/g)
NP$_3$D-EP3-MAH	2.2 ($\pm$ 0.01) $\times$ 10^{-5}	1.8 ($\pm$ 0.1) $\times$10^{-1}
NP$_3$D-EP4-MAH	3.1 ($\pm$0.06) $\times$ 10^{-5}	8.6 ($\pm$ 0.8) $\times$10^{-2}
NP$_3$D-EP5-MAH	3.5 ($\pm$0.04) $\times$ 10^{-5}	8.8 ($\pm$ 0.4) $\times$10^{-2}
NP$_3$D-EP6-MAH	2.4 ($\pm$0.02) $\times$ 10^{-5}	1.4 ($\pm$ 0.1) $\times$10^{-1}
NP$_3$D-EP7-MAH	3.3 ($\pm$0.02) $\times$ 10^{-5}	9.0 ($\pm$ 0.3) $\times$10^{-2}
PIB-PEHA	2.3 ($\pm$0.2) $\times$ 10^{-4}	3.7 ($\pm$ 0.4) $\times$10^{-2}
PIB-DETA	7.4 ($\pm$0.7) $\times$ 10^{-4}	1.2 ($\pm$ 0.1) $\times$10^{-2}

The parameters listed in Table 4.2 describe the binding of dispersant at low dispersant concentration when the first monolayer is being formed at the surface of the CBPs. The trends obtained in Table 4.2 indicate that the NP$_3$D-EPX-MAH samples form a monolayer on the CBP surface more efficiently than the PIBSI-based dispersants. This is certainly due to the larger size of individual EP coils which cover a larger area on the CBP surface than the size of shorter PIBSI-based dispersants allows. Adsorption of the NP$_3$D-EPX-MAH polymers buries some binding sites which become unaccessible. This effect is further enhanced by the multiple

attachment points distributed along the EP backbone under the form of NP_3D-Su groups. These groups ensure the efficient anchoring of the NP_3D-EPX-MAH samples on the CBPs surface, as demonstrated by the substantially larger binding constants obtained in Table 4.2. Since clustering enhances the ability of succinimide pendants to associate with other polar groups, the more clustered distribution of SAH pendants found for NP_3D-EP3-MAH and NP_3D-EP6-MAH promotes their stronger binding (largest K values) onto the CBPs.

CHAPTER 5: CONCLUSIONS

The seven maleated EP copolymer samples provided by DSM, namely EPX-MAH with X=1-7, constituted an invaluable set of samples to probe the effect that succinic anhydride (SAH) clustering has on the solution properties of these samples. These samples had similar molecular weight distributions with a number average molecular weight (M_n) of 40 ± 1 kg.mol-1 and a polydispersity index of 2.3 ± 0.2, so that differences in behavior could be attributed solely to differences in the distribution of the SAH pendants along the chains. The SAH content of the EPX-MAH samples was determined by FTIR absorbance on the pristine EPX-MAH samples and UV-Vis absorbance on the EPX-MAH samples after reaction with two aromatic compounds, namely 1-pyrenemethylamine and N-phenyl-p-phenylenediamine (NP$_3$D), that absorb in the UV-Vis spectrum. The SAH contents (λ_{SAH}) obtained from the three independent procedures were in reasonable agreement with each others, yielding values ranging from 158 ± 11 to 211 ± 2 μmol of SAH per gram of polymer. Thus, it could be concluded that the seven EPX-MAH samples had similar chemical compositions, as established in Chapter 3.

The main difference between the EPX-MAH samples was in the level of clustering exhibited by their SAH pendants. This parameter was inferred from absorption and fluorescence measurements on the pyrene-labeled polymers (Py-EPX-MAH) obtained from the reaction of EPX-MAH and 1-pyrenemethylamine (PMA). Pyrene derivatives possess photophysical features that are affected by pyrene aggregation. Upon pyrene aggregation, the absorption spectrum becomes broader, the fluorescence spectrum shows excimer emission, the excitation spectra of the pyrene monomer and excimer are shifted, and the excimer fluorescence decays display a reduced risetime. When these fluorescence experiments were applied to the Py-EPX-MAH samples, they indicated that samples Py-EP3-MAH and Py-EP6-MAH formed pyrene aggregates in polar THF as a result of more clustered distribution of the SAH pendants.

Since some redundancy was found with the seven EPX-MAH samples, some samples having similar SAH contents and SAH clustering levels, samples EPX-MAH with X=3-7 were selected out of the seven EPX-MAH samples to probe the effect that SAH clustering had on the solution properties of these polymers. The results of this study were described in Chapter 4. The solution property that was investigated first was the ability of the Py-EPX-MAH samples to self-associate in an apolar solvent. Hexane was selected as an apolar solvent and the emission and excitation fluorescence spectra of the Py-EPX-MAH samples were acquired in polar THF and hexane. Comparison of the fluorescence spectra demonstrated the enhanced pyrene excimer formation of the Py-EPX-MAH samples in hexane. This effect was attributed to intra- and interpolymeric association holding the Py-EPX-MAH chains together in hexane via dipolar interactions of the succinimide pendants. These interactions are strongly reduced in more polar THF, resulting in much reduced pyrene excimer formation. Furthermore, it was also found that SAH clustering led to stronger self-association of the Py-EPX-MAH samples in hexane.

Having applied fluorescence techniques to demonstrate at the molecular level that the succinimide pendants promote intra- and interpolymeric associations in apolar solvents, and that these interactions are further enhanced by SAH clustering, these effects were probed further at the macroscopic level by monitoring how the viscosity of Py-EPX-MAH samples would vary as a function of polymer concentration. The profiles of solution viscosity versus polymer concentration were presented in Figure 4.4. For all the Py-EPX-MAH samples, the profiles showed a much stronger viscosity increase with increasing concentration for the solutions in hexane. The profiles obtained for all Py-EPX-MAH samples overlapped in THF, confirming the lack of interpolymeric association taking place. In hexane, the two Py-EPX-MAH samples found to have a more clustered distribution of SAH pendants showed a much steeper viscosity increase

65

when compared to the viscosity profiles obtained with the three other samples. In particular, Py-EP3-MAH with a pyrene content larger than Py-EP6-MAH, showed the steepest increase in viscosity of all Py-EPX-MAH samples. Thus, it can be concluded that the interpolymeric associations undergone by the Py-EPX-MAH samples in hexane were promoted by polar interactions between the succinimide pendants, that these interactions were further enhanced for samples having a more clustered distribution of SAH pendants, namely for samples Py-EP3-MAH and Py-EP6-MAH, and that a higher SAH content led to stronger associations.

On the one hand, the results obtained by fluorescence and viscosity confirmed earlier trends correlating the level of SAH clustering with the self-association of just two other maleated EP (EP-MAH) copolymers in hexane[1] and expanded these results to a family of five polymers, namely the EPX-MAH samples with X=3-7. On the other hand, the effect that SAH clustering might have on the efficiency of modified EP-MAH copolymers to adsorb onto the surface of carbon-rich particles, namely carbon black particles (CBPs), had never been investigated. The five EPX-MAH samples with X=3-7 were reacted with NP$_3$D to cap the SAH groups and yield the corresponding set of five NP$_3$D-EPX-MAH samples. Their adsorption onto CBPs was characterized by analysing their Langmuir isotherm. The adsorption isotherms indicated multilayer formation at the surface of the CBPs, a behaviour that is different from that obtained for polyisobutylene succinimide (PIBSI) dispersants. The difference between the adsorption isotherms obtained for the PIBSI and NP$_3$D-EPX-MAH dispersants was attributed to the different molecular architecture of the dispersants. PIBSI dispersants with a polar core flanked by two apolar PIB chains can target each binding site at the surface of the CBPs. An NP$_3$D-EPX-MAH chain with its multiple anchoring sites distributed along the chain spreads over the surface of the particles burying along the way some of the binding sites on the CBP surface.

66

Consequently, the NP$_3$D-EPX-MAH samples formed a monolayer at the surface of CBPs much more efficiently than the PIBSI dispersants do as found from the adsorption experiments. SAH clustering enhanced the binding strength of NP$_3$D-EP3-MAH and NP$_3$D-EP6-MAH compared to the binding strength of the three other polymers. Furthermore, NP$_3$D-EP3-MAH with a larger NP$_3$D content than NP$_3$D-EP6-MAH exhibited the largest binding constant of all NP$_3$D-EPX-MAH samples. Finally, comparison of Figures 4.4 and 4.9 leads to the conclusion that the effect of SAH clustering on the adsorption of the NP$_3$D-EPX-MAH samples onto CBPs is much less pronounced than its effect the viscosity of the Py-EPX-MAH solutions in hexane.

The data presented in this thesis represent an in-depth description of the complex behavior of an important family of oil-additives, namely EP-MAH copolymers. The thesis gathers three sets of independent experiments that yield internally consistent results. The information obtained by fluorescence at the molecular level on the self-association of the polymer samples could be successfully correlated to the macroscopic behaviour of the polymer solutions probed by viscosity and adsorption measurements. The in-depth understanding provided by this work on the solution properties of EP-MAH copolymers will contribute to making this study a reference from which future investigations can be based.

A study of particular interest would characterize the interactions and possibly competition that result from the simultaneous use of EP-MAH and PIBSI-based dispersants. Such investigation can be conducted by labelling one of the polymers with pyrene and the other with NP$_3$D. Since both chromophores have distinct photophysical features, the composition of a mixture of Py-EP-MAH and NP$_3$D-PIBSI dispersants can be readily characterized by absorption measurements. How the interactions between the two types of dispersants affect the solution

viscosity and the adsorption of one of the dispersants onto CBPs could be easily characterized thanks to the basic information compiled in this thesis. In short, the work conducted in this thesis opens new venues of research in the field of commercial oil-additives.

APPENDICES

Figure A.1 describes the geometrical construction that was used to calculate the peak height value after correcting for a sloping base line passing through the points (x_1, y_1) and (x_2, y_2).
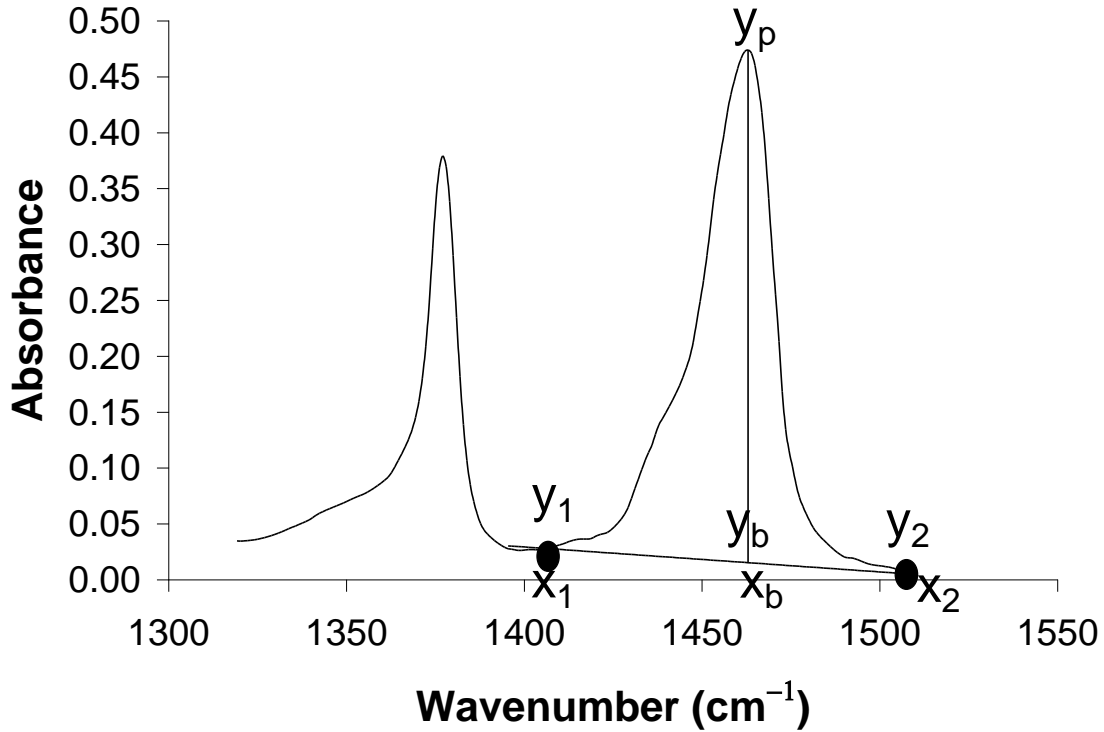
Figure A.1: Geometrical construction used to calculate the peak height value after correcting for a sloping base line.

y_b in Figure A.1 is obtained by applying Equation A.1.

$$y_b = \frac{(y_2 - y_1)}{(x_2 - x_1)} x_b + \frac{(y_1 x_2) - (y_2 x_1)}{(x_2 - x_1)} \tag{A.1}$$

The intensity after baseline correction is given by $y_p - y_b$ where y_p is the intensity at the peak maximum. This procedure was applied to generate the calibration curve shown in Figure 3.4D.

The area under the peak (A_p) shown in Figure A.1 was calculated by trapezoidal integration according to Equation A.2.

$$Ap = \frac{x_2 - x_1}{2n} (y_1 + y_2 + 2\sum_{i=2}^{n-1} y_i) \tag{A.2}$$

The area under the baseline (A_{BL}) in Figure A.1 is given by Equation A.3:

$$A_{BL} = (x_2 - x_1) y_1 - (x_2 - x_1) \frac{(y_2 - y_1)}{2} \tag{A.3}$$

The quantity A_p - A_{bL} yields the area under the curve shown in Figure A.1 corrected for a sloping baseline. This procedure was used to generate the calibration curve shown in Figure 3.4B.

Langmuir Isotherm Model

This thesis deals with the adsorption of polymers onto the surface of carbon black particles (CBPs) and how this adsorption is affected by changes in the nature of the polymers. This section presents a model that is used to describe the adsorption process.[1-2] It is based on the surface depicted in Figure B.1 where sites can be occupied or free.
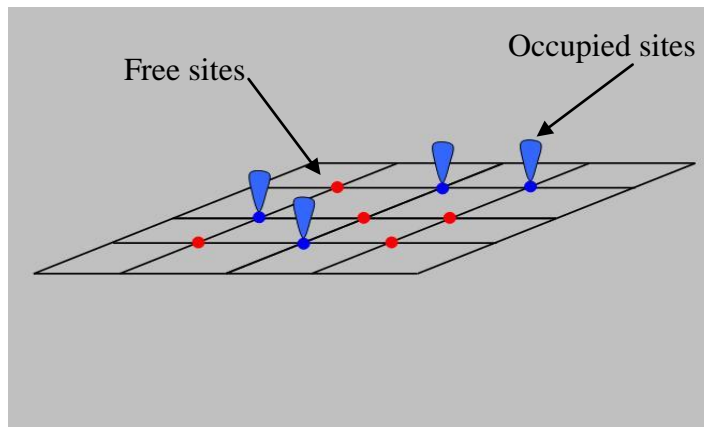
Figure B.1: Idealized surface which forms the basis of the Langmuir model. Containing free sites and already occupied sites.

In this thesis, the idealized surface is that of CBPs. The polymers represented by the symbols in Figure B.1 are adsorbed onto the surface. The surface consists of sites which are not yet occupied (Figure B.1) and sites which are already occupied by, in this case, polymers chains (Figure B.1). It is also assumed that each free site can be occupied by only one polymer chain. Polymers can adsorb or desorb from an occupied site. Adsorption is induced by attractive forces. A desorption process can be caused by an increase in the thermal energy. When the thermal

energy becomes larger than the binding energy, desorption dominates and little polymer remains adsorbed onto the surface.

A number of sites S are considered. Of those sites S, S_1 sites are occupied and S_0 sites are free where the population of the occupied and free sites is related to S according to Equation B.1.

$$S = S_0 + S_1 \tag{B.1}$$

When more sites are occupied, desorption is more likely to take place. This means that the number of desorption events is proportional to the number of occupied sites, so that the desorption rate is given by $k_1 \times S_1$, where k_1 is the desorption rate constant. At the same time the number of adsorption events is proportional to the number of free sites and the concentration C_{eq} of free polymer molecules, so that the adsorption rate is given by $k_2 \times C_{eq} \times S_0$, where k_2 is the adsorption rate constant. After a certain time the system reaches equilibrium and the rate of adsorption and desorption become equal. This observation leads to Equation B.2.

$$k_1 \times S_1 = k_2 \times S_0 \times C_{eq} = k_2 \times C_{eq} (S - S_1) \tag{B.2}$$

Equation B.2 can be simplified by introducing the fraction $\sigma = \dfrac{S_1}{S}$ of sites S occupied by polymer molecules and the adsorption equilibrium constant given by $K_{eq} = \dfrac{k_2}{k_1}$. Using these conventions, Equation B.2 can be rearranged into Equation B.3.

$$\sigma = \frac{K_{eq} \times C_{eq}}{1 + K_{eq} \times C_{eq}} \tag{B.3}$$

The fraction of the occupied surface can also be replaced by $\dfrac{\Gamma}{\Gamma_{max}}$ where Γ_{max} is the maximum

amount of polymer which can be adsorbed onto the surface and Γ is the amount of polymer

actually adsorbed. Equation B.4 is obtained by multiplying both sides of Equation B.3 by Γ_{max} .

$$\Gamma = \frac{\Gamma_{max} \times K_{eq} \times C_{eq}}{1 + K_{eq} \times C_{eq}} \tag{B.4}$$

Equation B.4 can be linearized by expressing $\dfrac{1}{\Gamma}$ as a function of $\dfrac{1}{C_{eq}}$ as done in Equation B.5.

$$\frac{1}{\Gamma} = \frac{1}{\Gamma_{max}} + \frac{1}{\Gamma_{max} \times K_{eq} \times C_{eq}} \tag{B.5}$$

According to Equation B.5, a plot of $\dfrac{1}{\Gamma}$ versus $\dfrac{1}{C_{eq}}$ results in a straight line whose slope and

intercept yield K_{eq} and Γ_{max}, respectively.

REFERENCES

Chapter 1

[1] Gurumayum, S.; Moreton, D.; Vicent, B.*Colloid Interface Sci.* **2003**, *263*, 343-349

[2] Cox, A.; Mogford, B.; Harley, S. *Colloids Surf. A* **2001**, *181*, 205-213.

[3] Kozak, D.; Moreton, D.; Vicent, B. *Colloids Surf. A: Physicochem. Eng. Aspects* **2009**, *347*, 245-250.

[4] Shen, Y.; Duhamel, J. *Langmuir* **2008**, *24*, 10665-10673.

[5] Delfau, J.; Michaud, L.; Barassin, A. *Combustion Sci. Tech.* **1979***, 20,* 165-172.

[6] Bittner, J.; Howard, J.; Palmer, B. *Soot in Combustion System and Its Toxic Properties,* J. Lahaye and G. Prado eds. Plenum, 1983, New York, pp. 95-97.

[7] Herd, C.; McDonald, G.; Hess, W. *Chem. Tech*. **1991**, *65*, 1-8.

[8] Battye, W.; Boyer, K. *T.G.Methods for improving global inventories of black carbon and organic carbon particulates*, Report No. 68-D-98-046, Prepared for U.S. Environmental Protection Agency, Research Triangle Park, NC, by EC/R Inc., Chapel Hill, NC, 2002.

[9] Hansen, J.; Sato, M.; Ruedy, R.; Lacis, A.; Oinas, V. *Proc. Natl. Acad. Sci.* **2000**, *97*, 9875-9880.

[10] (a) Gallopoulos, N. *Soc. Autom. Eng.* **1970***, SP Paper* No 700506; (b) Edmisten, W.; Peterson, J.; Sholts, R. *Soc. Autom. Eng*. **1970**, *SP Paper* No 700509.

[11 Spengler, J.; Sexton, K. *Science* **1983**, *221*, 9-17.

[12] Samet, J.; Spengler, J. *Indoor Air Pollution - A Health Perspective* eds. **1991** Johns Hopkins University Press. Baltimore, MD, 45-60.

[13] Shaub, H.; Kelemn, S. *SAE International Congress & Exposition,* **1992**, Detroit.

[14] Gwidon, W.; Batchelos, A. *Engineering Tribology,* 3rd Ed, Elsevier, London, 2005, pp.93-94.

[15] Tomlinson, A.; Danks, N,; Heyes, M. *Langmuir* **1997**, *13*, 5881-5893.

[16] Myers, D. *Surfactant Science and Technology,* 3rd Ed. Wiley, 2006, New York, pp. 345-532.

[17] Jeffrey H. *Surf. Sci. Ser.* **1989**, *33*, 67-88.

[18] (a) Gaylord, N. *Macromol. Sci.-Rev. Macromol. Chem Phys*. **1975**, *13*, 235-261; (b) Gaylord, N. *Chemtech* **1989**, *19*, 435-440.

[19] Thielf, C. Y.; Hayden, T.E. US 2010/ 010748A1.

[20] Boehm, P. *Carbon* **1994**, *32*, 759-769.

[21] Donnet, R.; Bamsal, M. *Carbon Black: Science and Technology*, Marcel Dekker, Inc., 1993, New York, chapter 2.

[22] Wiltzius, P. *Phys. Rev. Lett.* **1987**, *58*, 710-713.

[23] Weitz, D.; Huang, S.; Lin, Y. *Phys. Rev. Lett.* **1985**, *54*, 1416-1419.

[24] Bezot, P.; Hesse-Bezot, C. *Lubrication Sci.* **2001**, *13*, 301-311.

[25] Harwell, J. *Surf. Sci. Ser.* **1989**, *33,* 257-301.

[26] Pugh, R.; Fowkes, F. *Colloids Surf.* **1984**, *9*, 33-49

[27] Rosen, J. National Science Foundation (U.S), *Surface active agents- Congresses*, 1987.

[28] Adamson, A. *Physical Chemistry of Surfaces, 2nd Ed,* Interscience, 1967, Detroit, pp. 83-85.

[29] Trivedi, B.; Culberston, M.; *Maleic Anhydride, Plentum Press,* 2006, New York, Chapter 11.

[30] Van Duin, M.; Machado, A.; Covas, J. *Adv Polym Tech*. **2004**, *23*, 196-210.

[31] Yasutomi, S.; Maeda, Y.; Maeda, T., *Ind. Eng. Chem. Prod. Res. Dev*. **1981**, *20,* 530-536.

[32] Samay, G.; Nagy, T.; White, B. *J. Appl Polym. Sci.* **1995**, *56*, 1423-1432.

[33] Volpert, E.; Selb, J.; Candau, F. *Macromolecules* **1996**, *29*, 1452-1463.

[34] Jimenex-Regalado, E.; Selb, J.; Candau, F. *Langmuir* **2000**, *16*, 8611-8621.

[35] Zhang, M.; Duhamel, J. *Macromolecules* **2004***, 37,* 1877-1890.

Chapter 2

[1] ASTM D6474 *Annual Book of ASTM Standards,* **2006**.

[2] David, R. *Handbook of Chemistry and Physics, Lide Ed.,* 77th Ed, 1997, Boca Raton, pp. 8.62-8.63.

[3] Zhang, M., Duhamel, J.; van Duin, M.; Meessen, P. *Macromolecules* **2004**, *37,* 1877-1890.

[4] 1-Pyrenemethyl succinimide was prepared by Jamie Yip, a former graduated student in Duhamel's laboratory.

Chapter 3

[1] Liu, N.; Russel, K.; Baker, W. *J. Appl. Polym. Sci*. **1990***, 41,* 2285- 2292.

[2] Samay, G.; Nagy, T.; White, B. *J. Appl. Polym. Sci*. **1995**, *56*, 1423-1437.

[3] Vito, G.; Lanzetta, N.; Maglio, G.; Malinconico, M.; Musto,P.; Palumbo, R. *J.*

Polym. Sci.: Polym. Lett. Ed. **1982**, *20*, 481-492,

[4] Gaylord, N.; Metha, M. *J. Polym. Sci.: Polym. Lett. Ed*. **1982**, *20*, 523-538.

[5] De Roover, B. *J. Polym. Sci. A: Polym. Chem.* **1995**, *33*, 829-842.

[6] Zhang, M.; Duhamel, J. *Macromolecules* **2004***, 37,* 1877-1890.

[7] Winnik, F. *Chem. Rev.* **1993**, *93*, 587-614.

[8] Kanagalingmam, S.; Ngan, C.; Duhamel, J. *Macromolecules* **2002**, *35*, 8560-8570.

[9] Duhamel, J. in *Molecular Interfacial Phenomena of Polymers and Biopolymers*
     Editor: P. Chen, Woodhead Publishing Limited, Cambridge, 2005, pp. 214-248.

[10] Turro, J.; Yekta, A. *J. Am. Chem. Soc.* **1978**, *100*, 5951-5952.

[11] a) Demas, J. N. *Excited State LifetimeMeasurements*; Academic Press: New York,
     1983.

 [12] Birks, J. B. *Photophysics of Aromatic Molecules*; Wiley: 1970, New York, pp 351.

[13] Zhang, M.; Duhamel, J. *Macromolecules* **2005***, 38,* 4438-4446.

[14] Lakowicz, J. *Principles of fluorescence spectroscopy*, 2nd ed, Kluwer Academic/
     Plenum Publishers, 1999, New York, Chapter 2.

[15] Costa, T.; Seixas de Melo, J.; Burrows, H. *J. Phys. Chem. B*. **2009***, 113*, 618-626.

Chapter 4

[1] Zhang, M.; Duhamel, J. *Macromolecules* **2004***, 37,* 1877-1890.

[2] Duhamel, J. *Molecular Interfacial Phenomena of Polymers and Biopolymers* Editor:
     P. Chen, Woodhead Publishing Limited, 2005, Cambridge, pp. 214-248.

[3] Zhang, M.; Duhamel, J. *Macromolecules* **2005***, 38,* 4438-4446.

[4] Kozak, D.; Moreton, D.; Vicent, B.; *Colloids Surf. A: Physicochem. Eng. Aspects* **2009**, *347*, 245-250.

[5] Shen, Y.; Duhamel, J. *Langmuir* **2008**, *24*, 10665-10673.

[6] Won, Y.: Meeker, S.; Trapped, V.; Weitz, D. *Langmuir* **2005**, *21*, 924-932

[7] Dubois-Clochard, M.; Durand, J.; Delfort, B.; Gateau, P.; Barre, L.; Blanchard, I. *Langmuir* **2001**, *17,* 5901-5917.

[8] Selby, K. *SAE* **1998** No. 981369.

[9] Papke, B.; Robinson, M. *Langmuir* **1994**, *10*, 1741-1748.

[10] Chen, Y.; Xu, Z.; Israelachvilli, J. *Langmuir* **1992**, *8*, 2966-2972.

[11] Benfaremo, N.; Nalesnik, T. E. EO 0 396 297 B1 1995.

[12] Malandro, D. L.; Alessi, M. L. US 2007/0006855 A1 2007.

[13] Thiel. Y. C.; Hayden, T. E. US 2010/0107483 A1 2010.

[14] Butt, H.; Graf, K.; Kappl, M. Physics and Chemistry of Interfaces, *2nd Ed. Wiley-VCH, 2006,* Germany, pp.187-189.

[15] Adamson, A. *Physical Chemistry of Surfaces, 2nd Ed,* Interscience, 1967, New York, pp. 617-618.

CONCLUSIONS

[1] Zhang, M.; Duhamel, J. *Macromolecules* **2005***, 38,* 4438-4446.

APPENDIX

[1] Adamson, A. *Physical Chemistry of Surfaces*, 2nd Ed, Interscience, New York, 1967, Chapter XVII.

[2] Langmuir, I. *J. Am. Chem. Soc.* **1918**, *40*, 1361-1368.